PHILOSOPHICAL TRANSACTIONS OF THE ROYAL SOCIETY A MATHEMATICAL, PHYSICAL & ENGINEERING SCIENCES

Circular Islands as Resonators of Long-Wave Energy

W. Summerfield

Phil. Trans. R. Soc. Lond. A 1972 **272**, 361-402
doi: 10.1098/rsta.1972.0054

CIRCULAR ISLANDS AS RESONATORS OF LONG-WAVE ENERGY

By W. SUMMERFIELD†
Department of Earth and Planetary Sciences, The Johns Hopkins University, Baltimore, Maryland, U.S.A.

(*Communicated by O. M. Phillips, F.R.S. – Received 8 June 1971*)

CONTENTS

	PAGE		PAGE
1. Introduction	362	7. Cylindrical symmetry; the general case	392
2. Mathematical formulation	363	8. Further discussion; an application	395
3. Free waves around the island	365	Appendix A. Straight shelf investigation	396
4. Response at the coast to monochromatic radiation from the ocean	381	Appendix B. The rotation-induced 'beat-frequency'	400
5. The response at the coast to a travelling pulse	386	References	402
6. Effect of the Earth's rotation	390		

A study is made of the long gravity waves trapped around isolated, cylindrically symmetrical island–continental shelf topographies. Numerical evaluation of the discrete complex spectra of the trapped wave modes reveals that the oscillations are of two, essentially different kinds. The 'trapped-leaky' wave-modes are the analogue of the trapped (edge) wave-modes along straight shorelines and many of their properties, including the Coriolis split in frequency, are deducible from the simpler geometry. On the other hand, the 'shelf-island' modes have no counterpart in the motions trapped along extended shorelines; they are virtually generated in the ocean round a vertical-walled circular island of radius equal to that of the island-shelf system at the sea floor.

It is shown that the trapped wave-modes do not necessarily have the 'inner critical circle' property elucidated by Longuet-Higgins (1967) for the similar modes of oscillations of the waters over a circular seamount. On the other hand, the modes do have 'wave' domains adjacent to the coast whenever the undisturbed depth of water at the island's shoreline is zero; there may still be critical circles in the shallow water region over the continental shelf. For those islands where the water has non-zero depth at the shoreline, the computation verifies Longuet-Higgins's hypothesis (Longuet-Higgins 1967, § 13) concerning the affect on the trapped wave-modes of the presence of an island in the middle of the sea-mount.

It is also shown that the fundamental 'trapped-leaky' modes dominate the disturbance observed at the coast when plane wave radiation from the ocean interacts with the island-shelf system. For the particular example where the excitation has the form of a rectilinear pulse, it is shown that power spectra of the resulting oscillations exhibit some of the features of the spectra of real wave records made at islands following the passage of tsunamis.

† Present address: Dept. of Mathematics, University of Papua and New Guinea, Boroko, T.P.N.G.

Vol. 272. A. 1225. (Price £1.10; U.S. $3.10) 33 [Published 8 June 1972

1. Introduction

Close scrutiny of surface wave data from islands has, in some instances, lead to the suggestion that the unbounded waters around such features have natural periods. In recent, independent investigations, Longuet-Higgins (1967) and Shen, Meyer & Keller (1968) show how free modes of oscillation may be possible, owing to the phenomenon of wave refraction. The modes consist of waves which are guided around the island by the bottom contours of the surrounding sea-bed the waves being effectively trapped in the shallow near-shore water as a result of wave refraction in the steep continental slope region; there exists a discrete set of resonance frequencies, determined by the requirement that the waves remain in phase after the complete circuit. However, such a description glosses over the difficulties inherent in mathematical analyses of waves in water near shores, where progress has usually been dependent on the introduction of suitable approximations. In this example, the authors choose quite different approaches. Longuet-Higgins bases his analysis on the linear shallow-water theory of waves, whereas Shen *et al.* develop an approximate theory based on the smallness of the sea-bed slope; the latter leads to the geometrical optics theory of surface waves of Keller (1958). Nevertheless, there is remarkable agreement in the results where overlap occurs, especially with respect to the characteristics of the free wave-modes (see Shen *et al.* for a full discussion). In particular, both authors show that the motions must leak energy from the shallow-water region to the open ocean whenever the latter has finite depth. But, in its present form, the method of analysis of Shen *et al.* does not permit computation of the dissipation rates. On the other hand, Longuet-Higgins evaluates the complex eigenfrequencies of the oscillations for a model circular sea-mount, verifying that the 'topography-induced' leakage of energy may be exceedingly slow for some modes. However, Shen *et al.* readily extend their investigation to topographies where an island sits on top of the sea-mount, in contrast with Longuet-Higgins who infers what the effect will be (of such an island on possible free wave-modes) from the profiles of the oscillations for the sea-mount model. Finally, Shen *et al.* (1968) restrict attention to cylindrically symmetrical topographies, whereas Longuet-Higgins (1967) discusses the effects of a non-circular shape on the frequencies of the free modes, and points out conditions under which free modes may be expected for more general bottom topography.

We also note that the authors use the term 'trapping' in different senses. Longuet-Higgins only calls those free modes of oscillation where the leakage of energy from the shallow-water region is extremely small, 'trapped modes'. Shen *et al.*, use the terminology in a more formal sense to refer to the wave pattern, not the wave energy.

In this paper, we examine in more detail the 'topography-induced' leakage of energy for the free wave motions around cylindrically symmetrical island–continental shelf topographies. We adopt the shallow-water theory of waves as the basis of our investigation, noting that the studies by Shen *et al.* (1968) and Longuet-Higgins (1967) are in substantial agreement for the lowest modes in the spectra of waves over a circular sea-mount. This simplication permits computation of the complex eigenfrequencies. However, it should be pointed out that application of the results may be limited, for it is well known that shallow-water theory yields an adequate description of the properties of small amplitude waves of frequency σ, propagated in water of uniform depth h_2, provided $\sigma^2 h_2/g < \frac{1}{3}$ say, where g is the acceleration due to gravity. With $\sigma^2 h_2/g$ written in terms of the dimensionless frequency ν and parameter ϵ introduced in § 3, it is seen (§ 3) that our analysis may be restricted to those free wave-modes where $\epsilon\nu < 0.6 a_2/h_2$; a_2 is the radius of the island-shelf

complex at the sea floor, and h_2 is the depth of the ocean. With $a_2 = 30\,\text{km}$ and $h_2 = 4\,\text{km}$, $0.6a_2/h_2 \doteqdot 5$. To look ahead, it will be seen that the investigation is at least valid for the most important free wave-modes, the fundamental modes at small n; n is the dimensionless azimuthal wavenumber, which takes only integral values. On the other hand, the application of the results to real islands will be merely limited to those oscillations with periods greater than 5 min.

First, we focus attention on the particular case where the circular island is surrounded by a continental shelf of uniform width and depth, and where the continental slope is a discontinuity in the depth. Although not oceanographically realistic, the model has the advantage that one can readily deduce the properties of the free wave-modes from their analytic representation; further, the limiting case where the island has zero radius is the circular sea-mount already investigated by Longuet-Higgins (1967). It is shown in § 3 that the dimensionless eigenfrequencies ν can be evaluated when numbers are assigned to n and the two parameters ϵ and α, where ϵ is the square root of the ratio of the depths of water on and off the continental shelf, and α the ratio of the radius of the island to that of the shelf. The computation reveals that the presence of the island on the underlying sea-mount does not introduce any further free modes of oscillation than those which can exist over the sea-mount when the island is absent. The computation also reveals that there are two essentially different kinds of free wave-mode, one of which is, as expected, analogous to the trapped (edge) wave-modes along straight coastlines (appendix A). Members of this class are called *almost trapped* (the terminology of Longuet-Higgins 1967) when the topography-induced leakage of energy is negligible; otherwise, they are termed 'leaky' modes. As might be expected, the magnitude of the energy dissipation is found to be critically dependent on the angle at which the mode's wave components on the shelf meet the continental slope; the leakage is extremely small when the angle of incidence is greater than the critical angle (cf. Longuet-Higgins 1967).

In § 7, we consider how far the results can be generalized to other topographies displaying cylindrical symmetry. It is seen that much can be said, particularly concerning the fundamental trapped wave-modes once it is noted that their dimensionless eigenfrequencies are the roots of the derivatives of Hankel functions whenever the continental shelf region is virtually non-existent.

In the intervening sections, a study is made of the disturbance observed at the shoreline due to plane wave radiation from the ocean striking the island-continental shelf system. The excitation has the form of a simple harmonic wave in § 4, and the form of a pulse in § 5.

In § 6, we investigate the influence on the *almost trapped* modes of the Coriolis forces due to the rotation of the earth.

Finally, in § 8, we seek evidence of the existence of the free modes of oscillation in wave records made at islands following the passage of tsunamis.

2. Mathematical formulation

Let r and θ be polar coordinates in the plane, undisturbed water-surface, centred on the circular island of radius a_1 (figure 1), and let $h(r, \theta)$ denote the undisturbed depth of fluid. Our island-shelf complex is modelled by the function

$$h(r,\theta) = \begin{cases} h_1, a_1 < r < a_2, \\ h_2, r > a_2, \end{cases} \tag{2.1}$$

where $a_2 (> a_1)$, h_1 and $h_2 (> h_1)$ are constants. Around the island, there is an annular shallow-water region of uniform depth h_1, which is contiguous with the deep water of depth h_2 across the

discontinuous change in depth at $r = a_2$. In the following sections, the shallow and deep-water regions will be referred to, respectively, as the *shelf* and the *ocean*, the discontinuity at $r = a_2$, as the *edge*, and the vertical wall at $r = a_1$, as the *coast*.

Let $\zeta(r, \theta, t)$ and $\boldsymbol{u}(r, \theta, t)$ denote, respectively, the vertical displacement of the free surface and the vector horizontal velocity of the fluid. On eliminating $\boldsymbol{u}$ from the linearized, shallow-water equations of motion for the non-rotating, inviscid, homogeneous fluid

$$\partial \boldsymbol{u}/\partial t = -g.\nabla\zeta, \tag{2.2}$$

and the equation of continuity

$$\partial\zeta/\partial t + \nabla.(h\boldsymbol{u}) = 0, \tag{2.3}$$

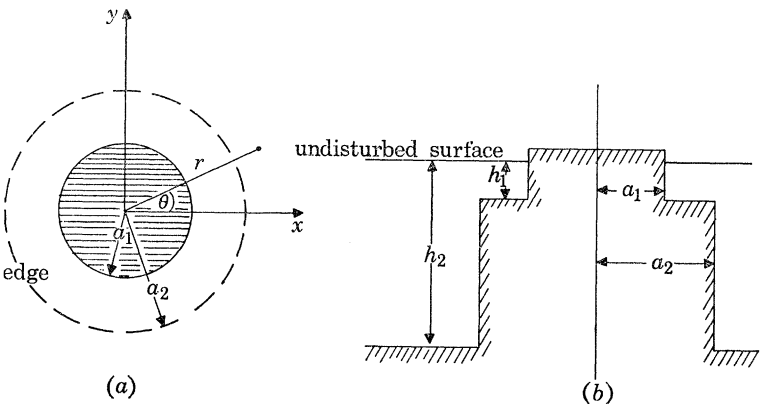

FIGURE 1. Circular island with shelf: (*a*) plan view, with island shaded in and edge denoted by broken circle; (*b*) radial cross-section.

where ζ has been assumed small in magnitude compared with h, one finds that ζ must satisfy the equation

$$\left[\nabla.h\nabla - \frac{1}{g}\frac{\partial^2}{\partial t^2}\right]\zeta = 0, \tag{2.4}$$

for all $r > a_1$, where

$$\nabla.h\nabla \equiv \frac{1}{r}\frac{\partial}{\partial r}\left(rh\frac{\partial}{\partial r}\right) + \frac{1}{r}\frac{\partial}{\partial\theta}\left(\frac{h}{r}\frac{\partial}{\partial\theta}\right).$$

With h given by (2.1), and the motion assumed simple-harmonic in time, the last equation simplies to the Helmholtz equations

$$[\nabla^2 + k_i^2]\,\zeta_i^* = 0 \quad (i = 1, 2), \tag{2.5}$$

where

$$\zeta(r, \theta, t) = \zeta^*(r, \theta)\,\mathrm{e}^{-\mathrm{i}\sigma t},$$

$$\nabla^2 \equiv \frac{\partial^2}{\partial r^2} + \frac{1}{r}\frac{\partial}{\partial r} + \frac{1}{r^2}\frac{\partial^2}{\partial\theta^2},$$

$$k_i = \sigma/(gh_i)^{\frac{1}{2}} \quad (i = 1, 2), \tag{2.6}$$

and where the suffix notation has been introduced to associate ζ_i^* with the region in which $h = h_i$. The separated-variable solutions of (2.5) are well known. In this investigation, the functions of the radial coordinate will be the Bessel functions of the third kind (Hankel functions)

$$H_n^{(1)} = J_n + \mathrm{i}Y_n, \quad H_n^{(2)} = J_n - \mathrm{i}Y_n, \tag{2.7}$$

where J_n and Y_n are, respectively, those of the first and second kinds. The reader is referred to Longuet-Higgins (1967, § 5) for a study of these functions very relevant to the analysis of this paper.

At the edge, it shall be required that

$$\zeta_1(a_2, \theta, t) = \zeta_2(a_2, \theta, t), \tag{2.8}$$

and that the normal component of the volume (mass) flux, $h\boldsymbol{u}\cdot\boldsymbol{n}$, also be continuous, where $\boldsymbol{n}$ is the unit normal to the discontinuity. Expressed in terms of ζ, the latter condition requires that (for all θ and t)

$$h_1 \frac{\partial \zeta_1}{\partial r} = h_2 \frac{\partial \zeta_2}{\partial r} \quad \text{at} \quad r = a_2. \tag{2.9}$$

Bartholomeusz (1958) has shown that the imposition of these conditions yields correct results for the reflexion coefficient of long waves normally incident on a straight step. Observational evidence (see, for example, Snodgrass, Munk & Miller 1962; Munk, Snodgrass & Gilbert 1964) suggests that shorelines are good reflectors of long, non-breaking waves of small amplitude. Accordingly, we require $\boldsymbol{u}\cdot\boldsymbol{n} = 0$ at the coast. The corresponding condition on ζ follows from (2.2), namely

$$\partial\zeta_1/\partial r = 0 \quad \text{at} \quad r = a_1. \tag{2.10}$$

Together with the differential equations (2.5) these boundary conditions determine the free modes of oscillation of the waters around the island; in the ocean, the solution must represent a wave motion propagated away from the edge because of the leakage of energy from the shelf.

3. Free waves around the island

Studies on the trapping of surface wave energy along extended coastlines and over submerged mountain ranges (see, for example, Munk *et al.* 1964; Garipov 1965; Buchwald 1969) suggest that the shallow-water region of the island-shelf system (2.1) can be regarded as a 'waveguide'. Comparison with waveguide mode theory in other fields (see, for example, Budden (1961) for that of radio waveguides) indicates that the most appropriate form of the expression for the free modes of oscillation will be

$$\zeta(r, \theta, t) = A \exp\{\mathrm{i}(n\theta - \sigma t)\} \begin{cases} \dfrac{H_n^{(2)\prime}(k_1 a_1)\, H_n^{(1)}(k_1 r) - H_n^{(1)\prime}(k_1 a_1)\, H_n^{(2)}(k_1 r)}{H_n^{(2)\prime}(k_1 a_1)\, H_n^{(1)}(k_1 a_2) - H_n^{(1)\prime}(k_1 a_1)\, H_n^{(2)}(k_1 a_2)} & (0 < a_1 < r < a_2), \\ \dfrac{H_n^{(1)}(k_2 r)}{H_n^{(1)}(k_2 a_2)} & (r > a_2), \end{cases} \tag{3.1}$$

where the prime denotes differentiation with respect to the argument, and n is integral in order that the solution be single valued in θ. The motion on the shelf is the sum of two systems of harmonic waves (at least, for large n and real σ), each of which propagates at the speed $(gh_1)^{\frac{1}{2}}$ of long waves in shallow water of depth h_1 along straight-line trajectories all tangent to the inner critical circle (terminology of Longuet-Higgins 1967, § 6) of radius $r = n/k_1$. The waves

$$A(\sigma) \exp\{\mathrm{i}(n\theta - \sigma t)\} H_n^{(1)}(k_1 r) \sim A(\sigma) \left(\frac{2}{n\pi \tan u}\right)^{\frac{1}{2}} \exp\{\mathrm{i}(n(\tan u - u) - \tfrac{1}{4}\pi + n\theta - \sigma t)\}, \tag{3.2}$$

where $\cos u = n/k_1 r$, with $k_1 r > n$, are directed towards the ocean, while the component motions

$$B(\sigma)\exp\{\mathrm{i}(n\theta-\sigma t)\}H_n^{(2)}(k_1 r) \sim B(\sigma)\left(\frac{2}{n\pi\tan u}\right)^{\frac{1}{2}}\exp\{\mathrm{i}(-n(\tan u-u)+\tfrac{1}{4}\pi+n\theta-\sigma t)\}, \quad (3.3)$$

are propagated towards the coast; $A(\sigma)$ and $B(\sigma)$ represent the additional terms in the expression (3.1). Provided $n/k_1 < a_2$, these wave trains are incident at the edge at the angle

$$\phi_i = \arcsin(n/k_1 a_2). \quad (3.4)$$

The integral constraint on n implies that the waves remain in phase after each complete circuit around the island. In the ocean, there is one system of waves propagated *away* from the island along straight trajectories tangent to the outer critical circle of radius $r = n/k_2$. The solution is illustrated in figure 2.

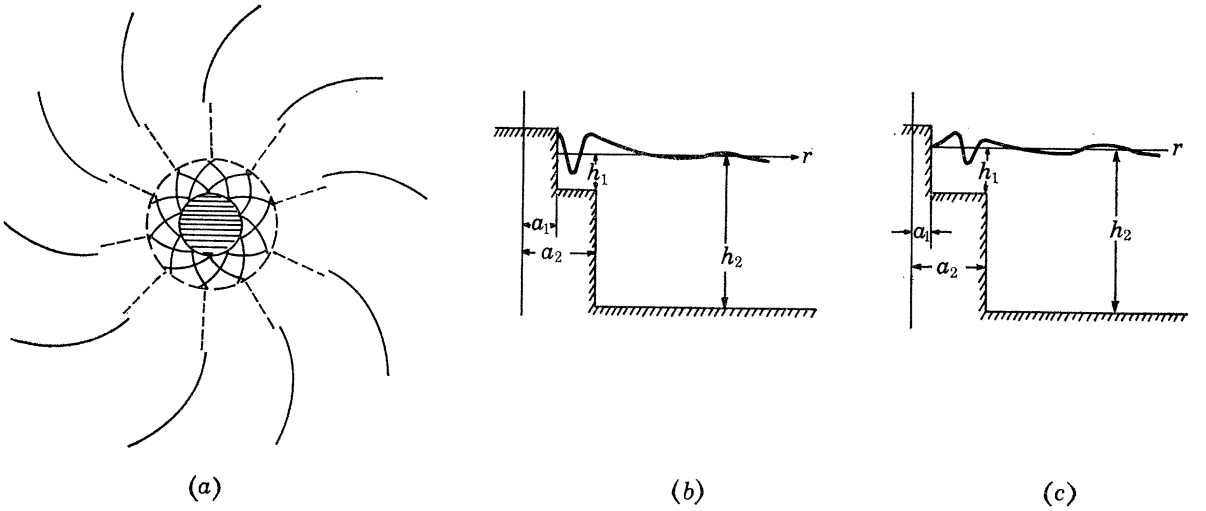

FIGURE 2. The form of free waves around the island: (*a*) plan view of the wave crests (full curves) when the waves on the shelf are reflected from the coast [$\alpha > \alpha_k$, defined by (3.20)]; (*b*) a radial section when $\alpha > \alpha_k$ (cf. figure 7); (*c*) a radial section when the inner critical circle is on the shelf, i.e. when $\alpha < \alpha_k$ (cf. figure 7).

The representation (3.1) meets all the conditions imposed on the solutions of (2.5), except (2.9). This latter condition requires that

$$(h_1/h_2)^{\frac{1}{2}}H_n^{(1)}(k_2 a_2)\,[H_n^{(1)\prime}(k_1 a_1)\,H_n^{(2)\prime}(k_1 a_2) - H_n^{(2)\prime}(k_1 a_1)\,H_n^{(1)\prime}(k_1 a_2)]$$
$$- H_n^{(1)\prime}(k_2 a_2)\,[H_n^{(1)\prime}(k_1 a_1)\,H_n^{(2)}(k_1 a_2) - H_n^{(2)\prime}(k_1 a_1)\,H_n^{(1)}(k_1 a_2)] = 0 \quad (a_1 \neq 0), \quad (3.5)$$

where, for an island-shelf complex of specified dimensions, the frequency σ is the only variable, and is a function of the parameter n. Thus, the eigenfrequencies of the free modes of oscillation are the roots of (3.5). Using known properties of the Bessel functions, it can be argued (Summerfield 1969) that these zeros cannot be real. Further, owing to the natural leak of energy to infinity, the motions are physically realistic only if they decay in time, i.e. σ must have a negative imaginary part. Hence we seek those zeros of (3.5) in the lower half of the complex σ plane. However, it proves advantageous to first examine the limiting cases of the model, when $a_1 = 0$ and when $a_1 = a_2$.

When $a_1 = 0$, the depth function (2.1) models the circular sill investigated in Longuet-Higgins (1967). The corresponding free mode expression and characteristic equation can be obtained from (3.1) and (3.5), respectively, in the limit where a_1 approaches zero with $r(> a_1)$ held fixed, on the

assumption that σ remains finite. The ocean part of the free mode expression is as given in (3.1), while that on the shelf becomes

$$\zeta(r,\theta,t) = A\exp\{\mathrm{i}(n\theta-\sigma t)\}.J_n(k_1r)/J_n(k,a_2);$$

the eigenfrequencies are given by the zeros of

$$(h_1/h_2)^{\frac{1}{2}}H_n^{(1)}(k_2a_2)\,J_n'(k_1a_2)-H_n^{(1)'}(k_2a_2)\,J_n(k_1a_2)=0. \tag{3.6}$$

The limit process suggests that, for models where $0<a_1\ll 1$, there exist eigenfrequencies of the motions (3.1) near (in the complex plane) those of the oscillations for the circular sill, $a_1=0$; the corresponding motions are little affected by the presence of 'small' islands on the underlying sill.

When $a_1=a_2$, the depth function (2.1) models a cylindrical island standing in water of uniform depth h_2. The ocean part of (3.1) is the appropriate free mode expression; (3.5) yields the corresponding characteristic equation,

$$H_n^{(1)'}(k_2a_2)=0. \tag{3.7}$$

Exact eigenfrequencies for the free modes of oscillation of the waters over the circular sill have been calculated (Longuet-Higgins 1967) in terms of the dimensionless frequency

$$\nu=\sigma a_2/(gh_1)^{\frac{1}{2}}, \tag{3.8}$$

for several values of the constant parameter

$$\epsilon=(h_1/h_2)^{\frac{1}{2}},$$

from its range
$$0<\epsilon<1, \tag{3.9}$$

where small (large) ϵ corresponds to a circular sill with large (small) differences in the depths of water at the edge. For our more general island-shelf complex, the eigenfrequencies can be computed in terms of these same dimensionless quantities, provided that a number is also assigned to the constant parameter

$$\alpha=a_1/a_2,$$

from its range,
$$0\leqslant\alpha\leqslant 1, \tag{3.10}$$

where $\alpha=0$ and 1 correspond, respectively, to the limiting circular sill and isolated, vertical-walled island models. Then we have from (2.6)

$$k_1a_2=\nu,\quad k_2a_2=\epsilon\nu,\quad k_1a_1=\alpha\nu, \tag{3.11}$$

and it follows that the dimensionless eigenfrequencies of the wave motions (3.1) are the zeros of

$$E(\nu;\epsilon,\alpha,n)\equiv\begin{cases}\epsilon H_n^{(1)}(\epsilon\nu)\,J_n'(\nu)-H_n^{(1)'}(\epsilon\nu)\,J_n(\nu) & (\alpha=0),\\ \epsilon H_n^{(1)}(\epsilon\nu).[H_n^{(1)'}(\alpha\nu)\,H_n^{(2)'}(\nu)-H_n^{(2)'}(\alpha\nu)\,H_n^{(1)'}(\nu)] & \\ \quad -H_n^{(1)'}(\epsilon\nu).[H_n^{(1)'}(\alpha\nu)\,H_n^{(2)}(\nu)-H_n^{(2)'}(\alpha\nu)\,H_n^{(1)}(\nu)] & (0<\alpha\leqslant 1),\end{cases} \tag{3.12}$$

in the lower half of the complex plane.

Now, $J_{-n}=(-1)^nJ_n$ and $H_{-n}=(-1)^nH_n$ (see, for example, Abramowitz & Stegun 1965). It follows that $E(\nu;\epsilon,\alpha,-n)$ and $E(\nu;\epsilon,\alpha,n)$ have identical roots, which implies that similar modes (3.1) can be propagated in either direction along the shelf, as one expects. Thus, we need only consider $n\geqslant 0$.

The cut in the complex ν plane associated with the Hankel functions in E will be taken along the negative imaginary axis. With the cut in this position, the roots of E in the lower left half-plane

reflect (in the cut) those in the lower right half-plane. Consequently, only the fourth quadrant need be searched for the roots of E. These zeros will be written in the form

$$\nu = \xi - \mathrm{i}\eta, \tag{3.13}$$

so that $\eta(>0)$ is the damping factor of the mode with frequency ξ.

One could evaluate the zeros of $E(\nu;\ \epsilon, \alpha, n)$ for particular island-shelf complexes (ϵ and α specified constants) by adopting a scheme of computation similar to that described in Longuet-Higgins (1967, § 6) for finding the roots of $E(\nu;\ \epsilon, 0, n)$; such an approach merely permits one to comment on the relative rates of damping of the various modes. On the other hand, the fact that equation (3.6) can be derived from (3.5) suggests that we regard the roots of $E(\nu;\ \epsilon, 0, n)$ as known, and proceed in the following manner with the computation. With n and ϵ held fixed, we take a zero of $E(\nu;\ \epsilon, 0, n)$ as the first approximation in Newton's rule for the numerical computation of roots of $E(\nu;\ \epsilon, \Delta\alpha, n)$, where $\Delta\alpha$ denotes a small positive increment; successive approximations rapidly converge on a root of $E(\nu;\ \epsilon, \Delta\alpha, n)$. We now take this newly computed zero of $E(\nu;\ \epsilon, \Delta\alpha, n)$ as the first approximation in Newton's rule for the evaluation of roots of $E(\nu;\ \epsilon, 2\Delta\alpha, n)$; convergence on a root of $E(\nu;\ \epsilon, 2\Delta\alpha, n)$ is again found to be rapid. By repeated use of this *step-by-step* process, we find that we can trace out in the complex plane, a curve (sequence) of the roots of E as α increases from zero (n and ϵ held fixed). We find that there is a similar curve of zeros attached to every root of $E(\nu;\ \epsilon, 0, n)$. Furthermore, each sequence is uniquely determined by the starting-point root of $E(\nu;\ \epsilon, 0, n)$ and the numbers assigned to ϵ and n, and can be traced through to any value of $\alpha < 1$. When α approaches 1, the *α-curve* of the zeros of E either tends to infinity or to a root of (3.7); in the latter case, the limit point is the zero of $H_n^{(1)\prime}(\epsilon\nu)$. Finally, by applying Rouché's theorem to the variation in the argument (computed numerically) of $E(\nu;\ \epsilon, \alpha, n)$ around the perimeter of the square $(0 < \xi < 50,\ 0 < \eta < 50)$, we find that every root of $E(\nu;\ \epsilon, \alpha, n)$ within the square can be accounted for by the step-by-step method of calculation.

Thus it appears that the presence of an island ($\alpha > 0$) on the immobilized, underlying sill (a_2, h_1, h_2 and hence ϵ, held fixed) of the model (2.1) does not introduce any further free modes of oscillation than those which can exist over the sill when the island is absent. Furthermore, an α-curve of the zeros of E traces the changing eigenfrequency of one particular mode, of constant wavenumber n/a_2 along the edge, caused by the island 'growing' (α increasing) on the underlying sill, from zero radius ($\alpha = 0$). We will see that much more can be deduced from the α-curves concerning the nature of the motions than just rates of decay; the interpretation is aided by the results of a similar study on the trapped wave-modes propagated along a shelf where the coast and edge are straight and parallel to each other (appendix A).

The remainder of this section is devoted to a detailed analysis of the free modes of oscillation.

The α-curve method of computation reveals that there are two types of trapped wave-mode (3.1), represented by different sets of the roots of E, and hence, of the zeros of $E(\nu;\ \epsilon, 0, n)$. The *first system* of the roots of $E(\nu;\ \epsilon, 0, n)$ (main sequence in the terminology of Longuet-Higgins 1967, § 6) contains an infinite number of members in one-to-one correspondence with the sequence of points

$$\nu = (\tfrac{1}{2}n + k + \tfrac{3}{4})\,\pi - \mathrm{i}\,\mathrm{arctanh}\,\epsilon \quad (k = 0, 1, 2, \ldots) \tag{3.14}$$

in the complex plane; the latter are the large ($|\epsilon\nu| \gg n$) analytical zeros of $E(\nu;\ \epsilon, 0, n)$. When ϵ is small, the one-to-one correlation is not altogether obvious, for those *first-system* roots of $E(\nu;\ \epsilon, 0, n)$ which are farthest (the left-hand, lowest frequency members) to the left of the line

$$\xi = n/\epsilon, \tag{3.15}$$

in the complex plane (figure 3) are much nearer the real axis than the values (3.14); see also figures 5 (*a*), 6 (*a*) of Longuet-Higgins (1967). The modes represented by these left-hand zeros have extremely slow leakage of energy to the ocean; the oscillations are *almost trapped* over the circular

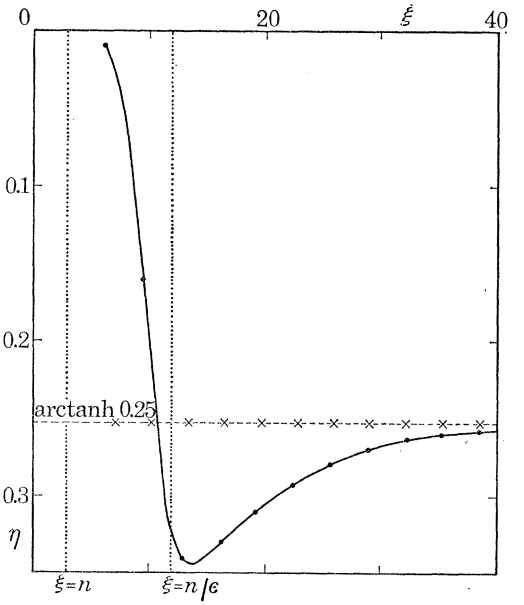

FIGURE 3. The one-to-one correlation for the *first system* roots of $E(\nu;\epsilon,0,n)$; the solid line joins the left-hand members of the *first-system* zeros (dots) of $E(\nu;0.25,0,3)$ and the dashed line, those of (3.14) (crosses) started at $k=0$. The roots of E representing *almost trapped* modes lie in the region between the lines $\xi=n$ and $\xi=n/\epsilon$.

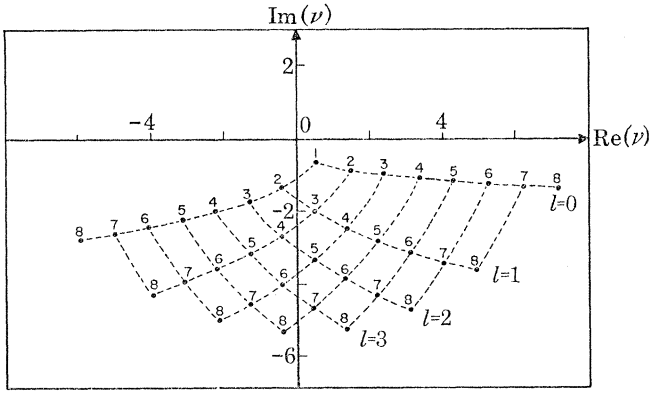

FIGURE 4. The n zeros of $H_n^{(1)\prime}(\nu)$, $n=0(1)8$, near the curve (in the complex plane) joining $\nu=n$ to $\nu=-n$ through $\nu=-$ i.n. 0.66274... (Olver 1954; also see Abramowitz & Stegun 1965). The zeros in the right half plane are denoted μ_{nl} where n is the order of the Hankel function and l has the value shown on the graph. Those zeros with Re $(\nu)<0$ lie on the sheet $-\frac{5}{2}\pi<\arg\nu<-\frac{1}{2}\pi$ of the Riemann surface.

sill. Modes represented by zeros farther to the right (ξ increasing) are wavelike both inside and immediately outside the edge and decay more rapidly in time.

The *second system* of the roots of $E(\nu;\epsilon,0,n)$ contains a finite number of members in one-to-one correspondence with the zeroes of $H_n^{(1)\prime}(\epsilon\nu)$. For convenience, the roots of $H_n^{(1)\prime}(\nu)$ on the sheet $-\frac{1}{2}\pi<\arg\nu<\frac{3}{2}\pi$ of the Riemann surface will be designated μ_{nl} where n is the order of the

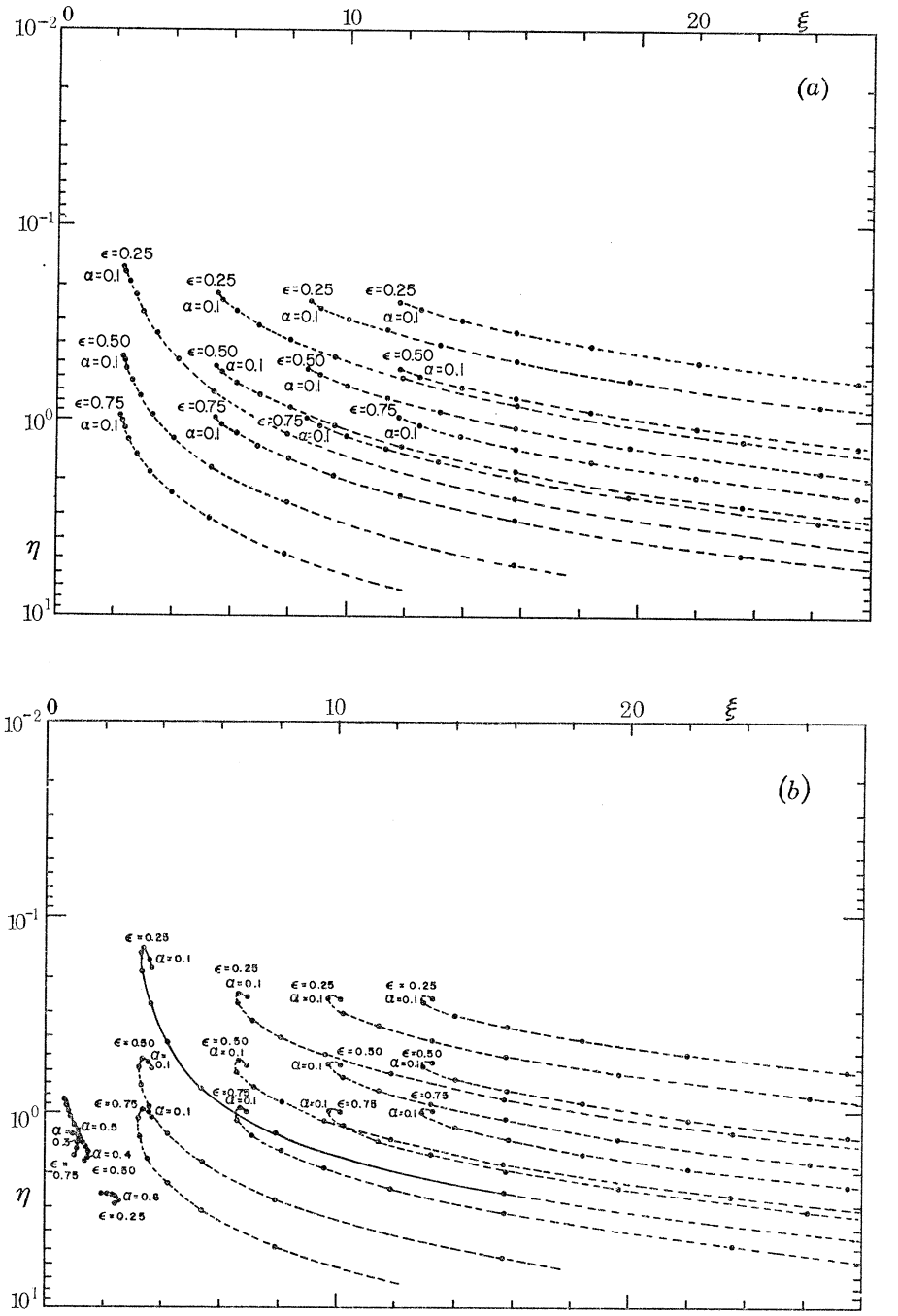

FIGURE 5. α-curves of the roots of $E(\nu;\ \epsilon = 0.25(0.25)0.75, \alpha, n = 0(1)7)$; note the logarithmic scale for η, compared to the linear scale of ξ. Each α-curve is labelled by its value of ϵ, usually near the starting-point $\alpha = 0.0$; the heavy dots on the curve are spaced at intervals of 0.1 in α, starting from $\alpha = 0.0$, with the first dot which can be plotted separately from that at $\alpha = 0.0$ also labelled. The portions of the α-curve which have been drawn as full lines, in general represent *almost trapped* modes. At larger values of α these curves are continued as broken lines. Other α-curves are broken lines for all α.

(a) α-curves of the roots of $E(\nu;\ \epsilon, \alpha, n = 0)$;
(b) α-curves of the roots of $E(\nu;\ \epsilon, \alpha, n = 1)$;
(c) α-curves of the roots of $E(\nu;\ \epsilon, \alpha, n = 2)$;
(d) α-curves of the roots of $E(\nu;\ \epsilon, \alpha, n = 3)$;
(e) α-curves of the roots of $E(\nu;\ \epsilon, \alpha, n = 4)$;
(f) α-curves of the roots of $E(\nu;\ \epsilon, \alpha, n = 5)$;
(g) α-curves of the roots of $E(\nu;\ \epsilon, \alpha, n = 6)$;
(h) α-curves of the roots of $E(\nu;\ \epsilon, \alpha, n = 7)$.

Hankel function and l has the value shown in figure 4 (cf. figures 5 to 7 (b) of Longuet-Higgins 1967). The corresponding root of $H_n^{(1)\prime}(\epsilon\nu)$ will be denoted

$$\epsilon_{nl} = \mu_{nl}/\epsilon; \tag{3.16}$$

then ϵ_{n0} is the root of (3.7) nearest to the real axis (having the smallest imaginary part).

We anticipate (cf. figure 3 with figure A 3 b) that the mode represented by the eigenfrequency of $E(\nu;\ \epsilon, 0, n)$ correlated with the kth point (3.14) resembles the kth ledge wave-mode (A 2) of

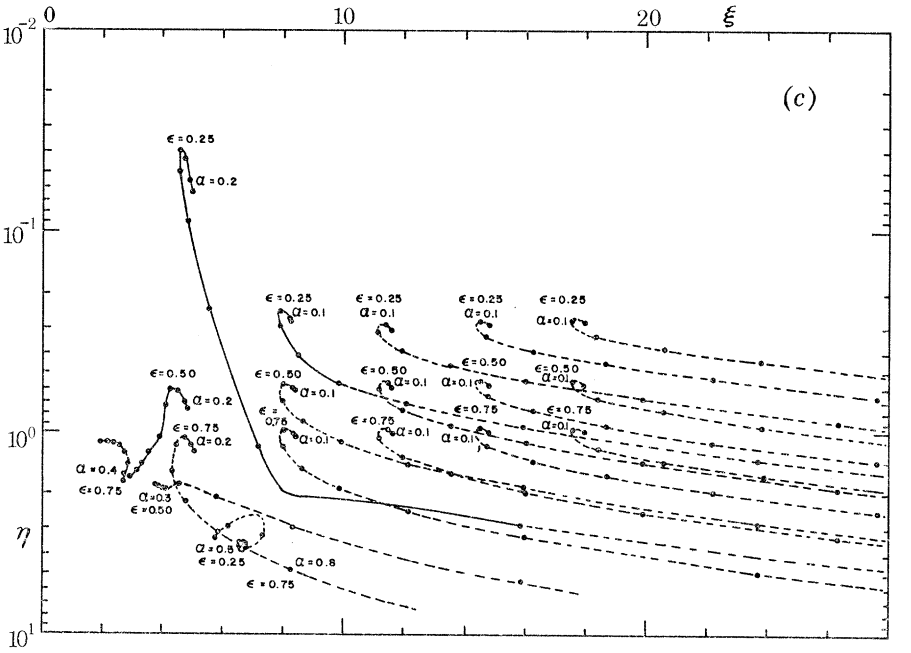

FIGURE 5 (c). For legend see p. 370.

wavenumber $m = n/a_2$ along the edge, and so has k nodal circles on the shelf. Then we expect the α-curve of the roots of E started on this eigenfrequency to follow a path in the complex plane similar to that traced out by the frequency of the kth ledge wave-mode as the width of the ledge goes to zero (appendix A). Thus, we anticipate that the α-curve started on the lowest frequency ($k = 0$) member of the *first system* of the roots of $E(\nu;\ \epsilon, 0, n)$ ends on ϵ_{n0}, and that the α-curve started on the jth ($j = k \geqslant 1$) member is asymptotic to the value (cf. (A 14))

$$\nu = \frac{(j-\frac{1}{2})\,\pi}{1-\alpha} - \mathrm{i}\frac{\operatorname{arctanh}\epsilon}{1-\alpha} \quad (j = 1, 2, 3, \ldots), \tag{3.17}$$

as α approaches 1; the latter are the large ($|\epsilon\nu| \gg n$, $|\alpha\nu| \gg n$) analytical zeros of

$$E(\nu;\ \epsilon, 0 < \alpha < 1, n).$$

Figure 5 plots, on a linear ξ, logarithmic η scale, a sufficient number of the α-curves started on *first-system* roots of $E(\nu;\ \epsilon = 0.25, 0, n = 0(1)\ 7)$ to verify this pattern, together with all the α-curves attached to the *second-system* roots of $E(\nu;\ 0.25, 0, n)$; the one-to-one correlation between the latter roots and the $\epsilon_{nl}(= \mu_{nl}/0.25)$ defined in (3.16) is clearly seen, for the zeros are close by and, with the exception of that nearest to ϵ_{n0}, joined to the ϵ_{nl} by α-curves in the limit $\alpha = 1$. Although figures 5 b, c show that, at $n = 1, 2$, the α-curve pattern for the *first-system* roots does not conform with that conjectured...for the α-curve emanating from the kth ($k \geqslant 0$) *first-system* root of

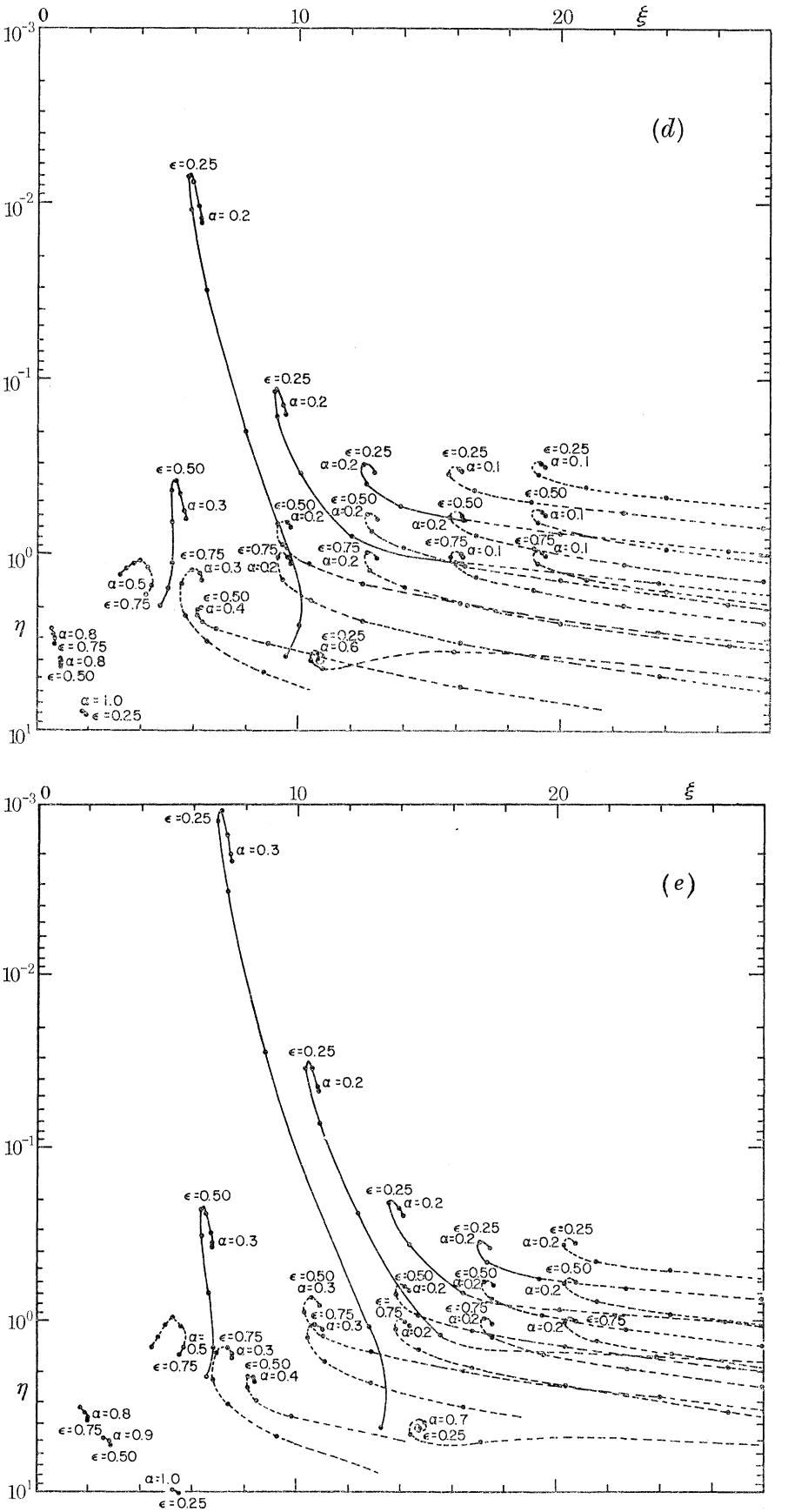

FIGURE 5 (*d*, *e*). For legend see p. 370.

PHILOSOPHICAL TRANSACTIONS OF THE ROYAL SOCIETY A MATHEMATICAL, PHYSICAL & ENGINEERING SCIENCES

$E(\nu; 0.25, 0, n)$ approaches the value (3.17) where $j = k+1$ when α tends to 1 ... close inspection of all the subfigures reveals that the postulated pattern evolves as n increases, with the *second-system* zero of $E(\nu; 0.25, 0, n)$ nearest to ϵ_{n0} supplying the 'missing' α-curve (a complete description is given in Summerfield (1969)). This latter point is clarified in figure 6, which replots the α-curves ending on ϵ_{n0}, in part (*a*), and those corresponding to $j = 1$ and 2 in (3.17), in part (*b*); α-curves emanating from roots of $E(\nu; 0.25, 0, 0)$ can be, and are, included in figure 6*b*. Accordingly, we introduce the notation that (cf. appendix A)

$$\nu_k = \xi_k - i\eta_k, \tag{3.18}$$

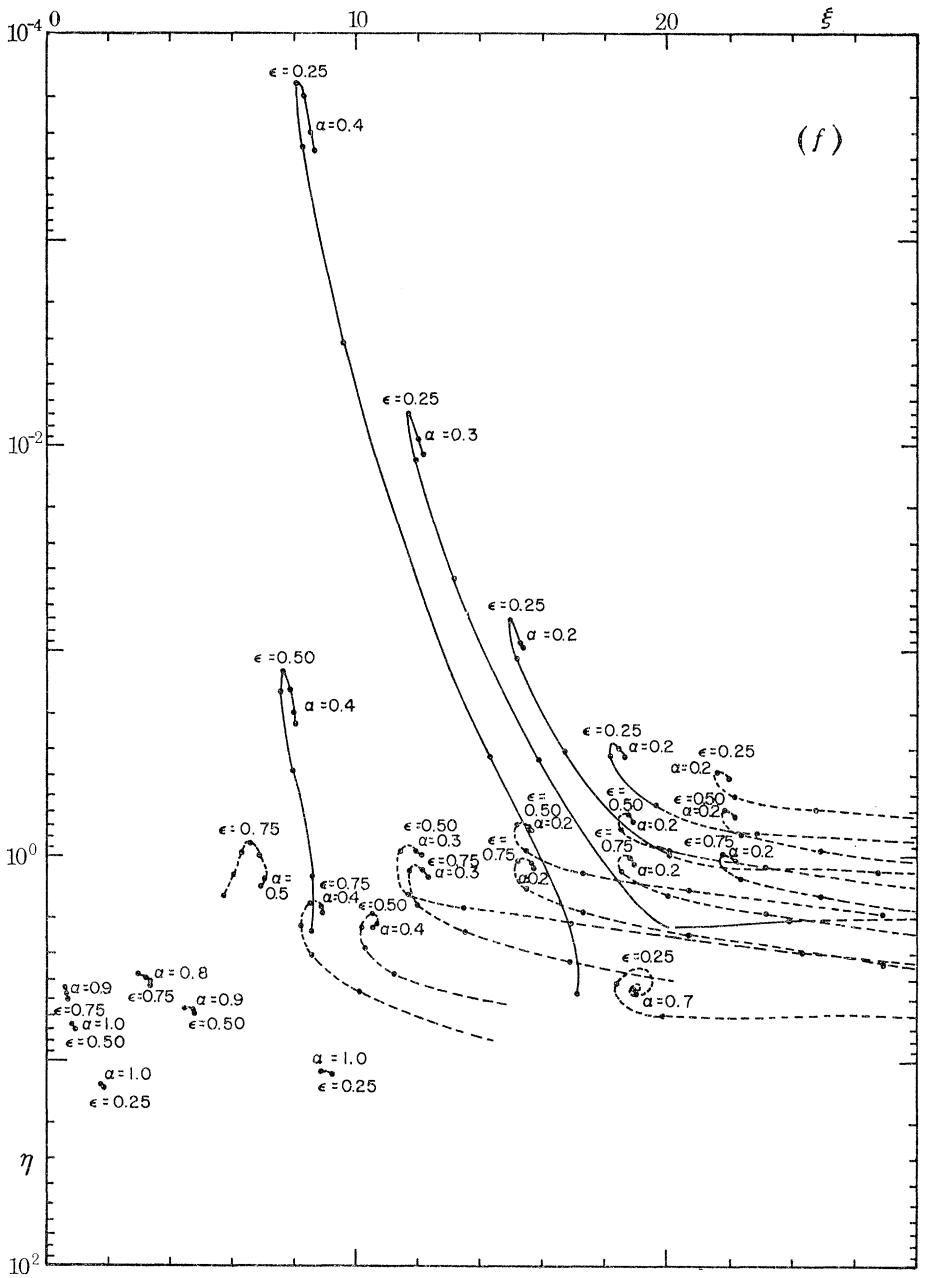

FIGURE 5 (*f*). For legend see p. 370.

denotes any eigenfrequency on the α-curve emanating from the kth ($\geqslant 0$) *first-system* root of $E(\nu; \epsilon < 2/\pi, 0, n)$; the limitation, $\epsilon < 2/\pi$, will become apparent later.

Confirmation that the mode represented by ν_k resembles the kth ledge wave oscillation (A 2) is provided by the free mode expression itself. In figure 7, there are plotted the radial cross-sections of (3.1) corresponding to the eigenfrequencies ν_0, ν_1 and ν_2 ($n = 5$, $\epsilon = 0.25$, α as shown in figure 7); note that the dimensionless radial variable

$$\rho = r/a_2, \tag{3.19}$$

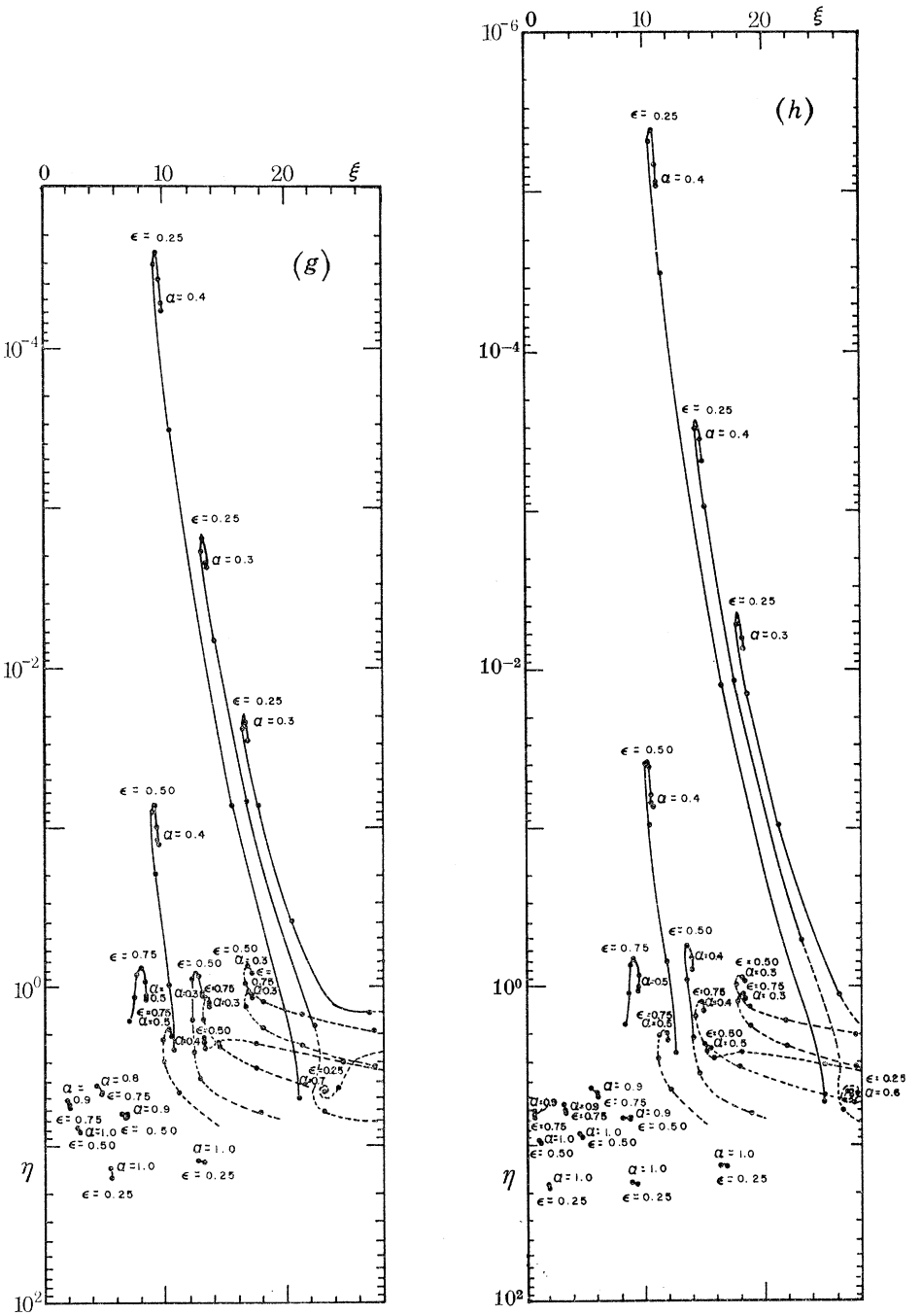

FIGURE 5 (g, h). For legend see p. 370.

has the range $\rho \geqslant \alpha$, where $\rho = \alpha$ at the coast, $\rho = 1$ at the edge, and $\rho > 1$ in the ocean. As expected, the profiles show, respectively, 0, 1 and 2 nodal circles (zero crossings) on the shelf. Furthermore, the profiles in figure 7*a* are for ν_k to the left of the line (3.15); figure 5*f* shows that

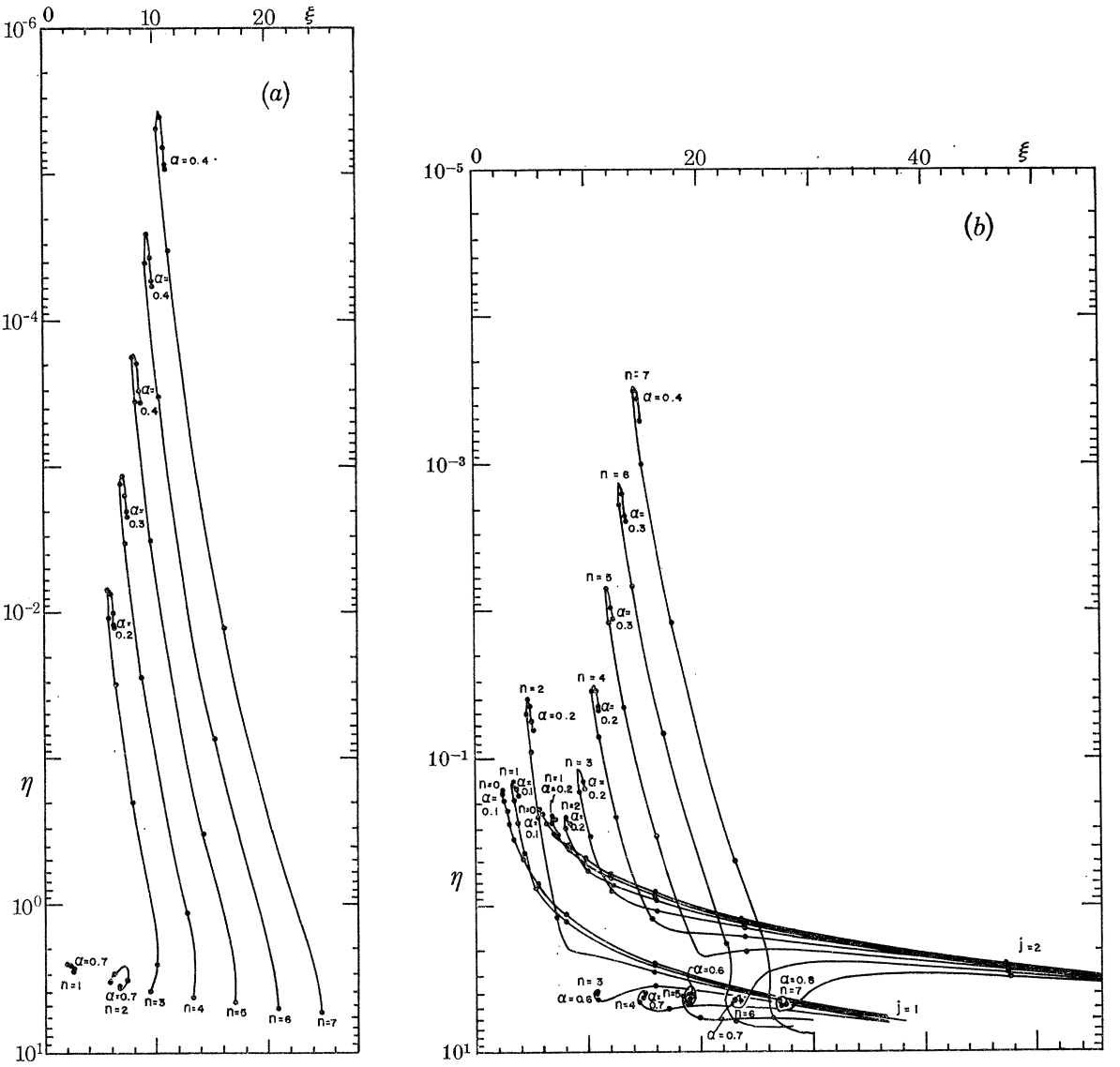

FIGURE 6. Clarification of the role of the α-curve of the zeros of E started on the root of $E(\nu; 0.25, 0, n)$ nearest to ϵ_{n0}, in the evolution (as n increases) of the α-curve pattern representing the 'trapped-leaky' modes; the dots on each α-curve have the same significance as in the previous figure. (*a*) The α-curves ending on ϵ_{n0}; (*b*) the α-curves which asymptote to the values (3.17) where $j = 1, 2$ when α approaches 1.0.

the modes have very small damping factors, and so are *almost trapped* on the shelf. One sees clearly the exponential decay in wave amplitude in the ocean, away from the edge out to the outer critical circle of radius $\rho = n/(\epsilon . \xi_k)$, characteristic of the perfectly trapped ledge wave oscillations (A 2). Table 1 records the values of the eigenfrequencies of the *almost trapped* modes (3.1) at $n = 5$, $\epsilon = 0.25$ for several α from its range (3.10), together with the similar values at $n = 3$ and $n = 7$.

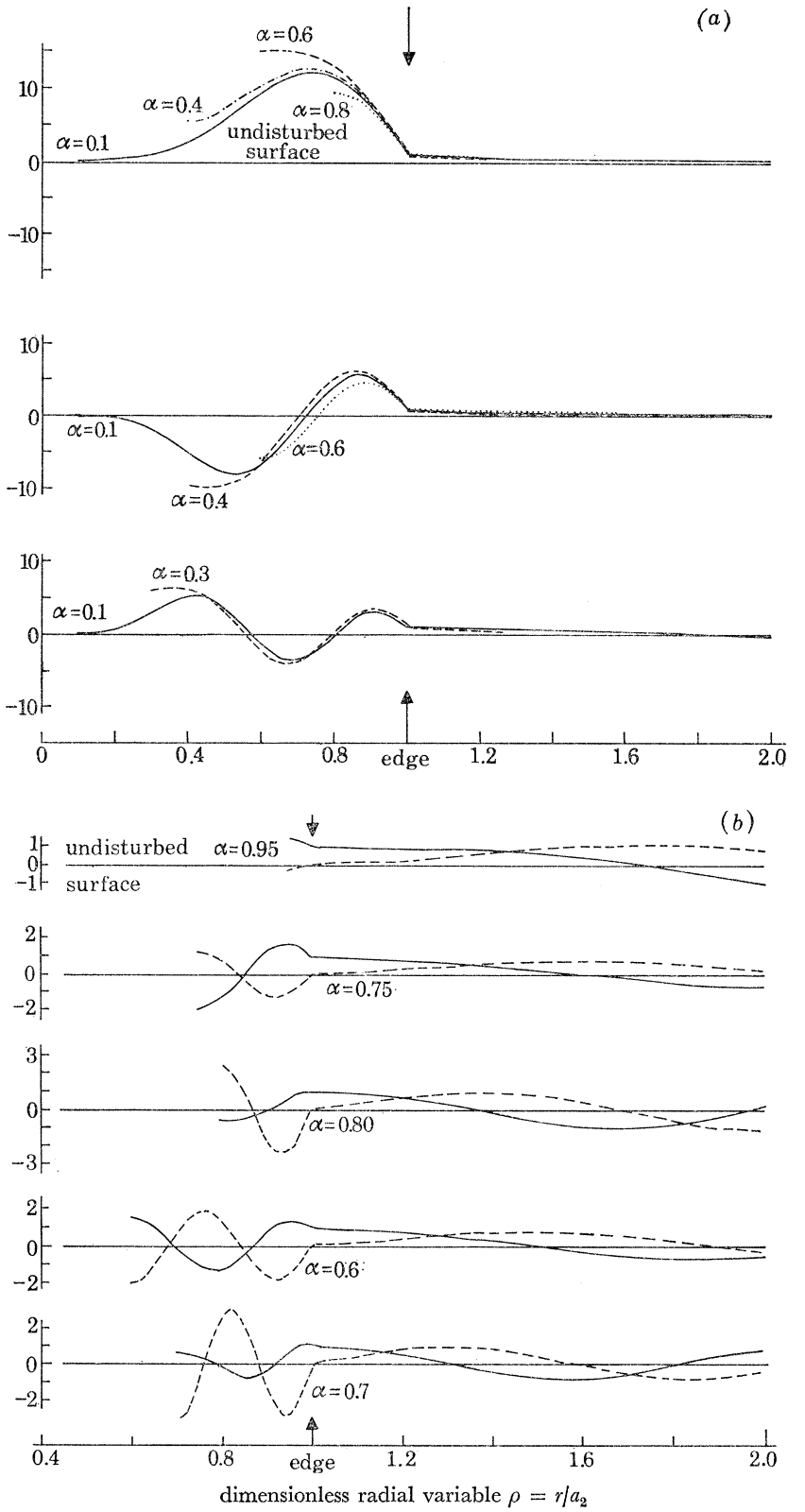

FIGURE 7. Radial sections of the wave form (3.1) for eigenfrequencies on the α-curves emanating from the 0, 1st and 2nd *first-system* roots of $E(\nu; 0.25, 0, 5)$. The values of α for which the profiles are plotted are marked on the appropriate graphs. (*a*) Graphs of the real part of the radial component of (3.1) for various ν_0 (top), ν_1 (middle) and ν_2 (bottom) to the left of the line (3.15) in the complex plane, e.g. at $\alpha = 0.4$ in the top figure,

$$\nu_0 = 8.556 - i0.0003$$

and at $\alpha = 0.3$ in the bottom figure, $\nu_2 = 14.9661 - i0.07099$ [see figure 5(*f*)]. The imaginary (90° out of phase) part of the radial component of (3.1) is, in all cases, virtually zero on the shelf. (*b*) Plots of the real (full curves) and imaginary (broken curves) parts of the radial component of (3.1) for ν_0 (top), ν_1 (centre two) and ν_2 (bottom two) at larger α. The ν_1 and ν_2 lie to the right of the line (3.15); the profiles show the 'leaky-wave' nature of the modes when the shelf is narrow.

TABLE 1. ACCURATE VALUES OF THE FREQUENCIES, RATES OF DAMPING, CRITICAL RADII, RESPONSE COEFFICIENTS AND ROTATION-INDUCED 'BEAT FREQUENCIES' FOR THE LOWEST ORDER *ALMOST TRAPPED* MODES (3.1) AT $n = 3, 5, 7$ AND $\epsilon = 0.25, 0.50$

α	frequency ξ_k	damping η_k	critical radii n/ξ_k	critical radii $n/\epsilon\xi_k$	Coriolis split in frequency (6.6)	$\lvert A_{nk}\rvert$	$\lvert B_{nk}\rvert$	coastal amplitude $\lvert A_{nk}\rvert$	max $\lvert B_n\rvert$ (4.9)
				$n = 3, \epsilon = 0.25$					
0.0	6.2092	0.1246×10^{-1}	0.48	1.93	0.0323	0.0579	0.0579	—	18.59
	9.4563	0.1566	0.32	1.27	0.0366	0.2055	0.2055	—	5.25
	12.8183	0.3383	0.23	0.94	−0.0222	0.3097	0.3097	—	3.66
0.1	6.2089	0.1246×10^{-1}	0.48	1.93	0.0324	0.0579	0.0579	0.0023	18.59
	9.4536	0.1561	0.32	1.27	0.0372	0.2050	0.2049	0.0280	5.25
	12.8030	0.3358	0.23	0.94	−0.0192	0.3083	0.3070	0.1025	3.66
0.2	6.1963	0.1215×10^{-1}	0.48	1.94	0.0365	0.0569	0.0569	0.0172	18.72
	9.3467	0.1401	0.32	1.28	0.0648	0.1898	0.1869	0.1852	5.34
	12.4542	0.3078	0.24	0.97	0.0610	0.2926	0.2797	0.5213	3.64
0.3	6.1049	0.1026×10^{-1}	0.49	1.97	0.0708	0.0506	0.0505	0.0470	19.70
	9.0407	0.1172	0.33	1.33	0.1588	0.1713	0.1685	0.3352	5.75
	12.5590	0.3945	0.24	0.96	0.0789	0.3458	0.3866	0.6811	3.92
0.4	5.8991	0.0753×10^{-1}	0.51	2.03	0.1565	0.0419	0.0418	0.0701	22.20
	9.1622	0.1630	0.33	1.31	0.1929	0.2230	0.2358	0.4342	5.78
	13.8647	0.5243	0.22	0.87	0.0326	0.3893	0.5468	0.6686	4.17
0.5	5.7404	0.0696×10^{-1}	0.52	2.09	0.2466	0.0426	0.0425	0.0861	24.45
	10.0302	0.3363	0.30	1.20	0.1775	0.3500	0.4515	0.6144	5.37
0.6	5.8337	0.1061×10^{-1}	0.51	2.06	0.3087	0.0612	0.0614	0.1190	23.16
	11.9990	0.7780	0.25	1.00	0.0571	0.5073	1.172	0.9534	6.02
0.7	6.4015	0.3065×10^{-1}	0.47	1.87	0.3402	0.1263	0.1300	0.2134	16.96
	15.9687	1.0945	0.19	0.75	−0.0152	0.4144	1.803	0.8379	6.59
0.8	7.0918	1.9837×10^{-1}	0.38	1.52	0.3734	0.3598	0.4727	0.5515	9.53
0.9	10.0200	25.2031×10^{-1}	0.30	1.20	0.5939	0.1276	9.100	1.152	14.44
				$n = 5, \epsilon = 0.25$					
0.0	8.6464	0.3613×10^{-3}	0.58	2.31	0.0154	0.0103	0.0103	—	114.4
	12.1245	0.1091×10^{-1}	0.41	1.65	0.0223	0.0537	0.0537	—	19.68
	15.3583	0.9563×10^{-1}	0.33	1.30	0.0331	0.1571	0.1571	—	6.57
0.1	8.6464	0.3613×10^{-3}	0.58	2.31	0.0154	0.0103	0.0103	0.0001×10^{-1}	114.4
	12.1245	0.1091×10^{-1}	0.41	1.65	0.0223	0.0537	0.0537	0.0003	19.68
	15.3582	0.9562×10^{-1}	0.33	1.30	0.0331	0.1571	0.1571	0.0026	6.57
0.2	8.6461	0.3611×10^{-3}	0.58	2.31	0.0154	0.0103	0.0105	0.0003	114.4
	12.1200	0.1083×10^{-1}	0.41	1.65	0.0231	0.0534	0.0534	0.0076	19.72
	15.3260	0.9239×10^{-1}	0.33	1.30	0.0379	0.1533	0.1528	0.0633	6.62
0.3	8.6373	0.3542×10^{-3}	0.58	2.32	0.0177	0.0102	0.0102	0.0020	115.0
	12.0059	0.0924×10^{-1}	0.42	1.67	0.0483	0.0478	0.0477	0.0397	20.66
	14.9661	0.7099×10^{-1}	0.33	1.34	0.1102	0.1304	0.1289	0.2101	7.26
0.4	8.5556	0.2996×10^{-3}	0.58	2.34	0.0424	0.0091	0.0091	0.0061	121.1
	11.6696	0.0692×10^{-1}	0.43	1.71	0.1385	0.0413	0.0413	0.0700	23.85
	15.1772	1.0719×10^{-1}	0.33	1.32	0.1404	0.1810	0.1885	0.2892	7.03
0.5	8.3137	0.1993×10^{-3}	0.60	2.41	0.1239	0.0070	0.0070	0.0097	141.4
	11.8728	0.1151×10^{-1}	0.42	1.68	0.1725	0.0628	0.0631	0.1003	21.92
	16.7166	3.0426×10^{-1}	0.30	1.20	0.1333	0.3297	0.4182	0.4521	5.50
0.6	8.0995	0.1729×10^{-3}	0.62	2.47	0.2238	0.0070	0.0070	0.0122	163.1
	13.1514	0.4457×10^{-1}	0.38	1.52	0.1648	0.1440	0.1499	0.1866	13.45
	20.0970	9.8305×10^{-1}	0.25	1.00	0.0192	0.5306	1.544	0.8688	6.28
0.7	8.3013	0.3529×10^{-3}	0.60	2.41	0.3009	0.0126	0.0126	0.0204	142.6
	15.8731	3.3892×10^{-1}	0.32	1.26	0.1877	0.3954	0.6022	0.4925	7.11
0.8	9.6061	3.1440×10^{-3}	0.52	2.08	0.3364	0.0512	0.0514	0.0665	65.39
	23.9041	20.4017×10^{-1}	0.21	0.84	−0.0816	0.2883	6.709	1.030	13.15
0.9	14.2944	324.3310×10^{-3}	0.35	1.40	0.3784	0.5407	0.9238	0.6536	11.39

TABLE 1 (*cont.*)

α	frequency ξ_k	damping η_k	critical radii n/ξ_k	critical radii $n/\epsilon\xi_k$	Coriolis split in frequency (6.6)	$\lvert A_{nk}\rvert$	$\lvert B_{nk}\rvert$	coastal amplitude $\lvert A_{nk}\rvert$	max $\lvert B_n\rvert$ (4.9)
			$n = 7, \epsilon = 0.25$						
0.0	10.9776	0.9025×10^{-5}	0.64	2.55	0.0102	0.00169	0.00169	—	747.7
	14.6605	0.4843×10^{-3}	0.48	1.91	0.0123	0.0116	0.0116	—	95.89
	18.0547	0.7339×10^{-2}	0.39	1.55	0.0167	0.0440	0.0440	—	23.96
0.1	10.9776	0.9025×10^{-5}	0.64	2.55	0.0102	0.00169	0.00169	0.0004×10^{-4}	747.7
	14.6605	0.4843×10^{-3}	0.48	1.91	0.0123	0.0116	0.0116	0.0002×10^{-2}	95.89
	18.0547	0.7339×10^{-2}	0.39	1.55	0.0167	0.0440	0.0440	0.0003×10^{-1}	23.96
0.2	10.9776	0.9025×10^{-5}	0.64	2.55	0.0102	0.00169	0.00169	0.0446×10^{-4}	747.7
	14.6604	0.4842×10^{-3}	0.48	1.91	0.0123	0.0116	0.0116	0.0208×10^{-2}	95.90
	18.0533	0.7324×10^{-2}	0.39	1.55	0.0169	0.0439	0.0439	0.0297×10^{-1}	23.97
0.3	10.9771	0.9013×10^{-5}	0.64	2.55	0.0103	0.00168	0.00168	0.6374×10^{-4}	748.0
	14.6458	0.4725×10^{-3}	0.48	1.91	0.0148	0.0114	0.0114	0.2575×10^{-2}	96.56
	17.9382	0.6371×10^{-2}	0.39	1.56	0.0357	0.0398	0.0398	0.2893×10^{-1}	24.97
0.4	10.9613	0.8692×10^{-5}	0.64	2.55	0.0139	0.00164	0.00164	3.662×10^{-4}	755.9
	14.4324	0.3484×10^{-3}	0.48	1.94	0.0609	0.0093	0.0093	0.9573×10^{-2}	106.8
	17.5544	0.5157×10^{-2}	0.40	1.60	0.1188	0.0371	0.0371	0.5821×10^{-1}	28.74
0.5	10.8293	0.6605×10^{-5}	0.65	2.59	0.0493	0.00137	0.00137	10.25×10^{-4}	826.4
	14.1314	0.3007×10^{-3}	0.50	1.98	0.1496	0.0093	0.0093	1.458×10^{-2}	123.5
	18.4340	1.4016×10^{-2}	0.38	1.52	0.1171	0.0732	0.0738	0.9272×10^{-1}	21.06
0.6	10.5110	0.4006×10^{-5}	0.67	2.66	0.1450	0.00103	0.00103	14.48×10^{-4}	1030.4
	14.8671	0.9407×10^{-3}	0.47	1.88	0.1600	0.0205	0.0205	2.667×10^{-2}	87.17
	21.0355	9.5122×10^{-2}	0.33	1.33	0.1135	0.2112	0.2320	2.170×10^{-1}	9.76
0.7	10.3927	0.4717×10^{-5}	0.67	2.69	0.2483	0.00132	0.00132	20.56×10^{-4}	1120.9
	17.4011	11.5293×10^{-3}	0.40	1.61	0.1457	0.0872	0.0883	8.819×10^{-2}	30.64
	26.0991	112.9711×10^{-2}	0.27	1.07	0.1617	0.5299	2.277	8.520×10^{-1}	8.06
0.8	11.2923	3.2098×10^{-5}	0.62	2.48	0.3231	0.00488	0.00488	62.74×10^{-4}	608.0
	23.0419	504.0856×10^{-3}	0.30	1.22	0.1992	0.4881	1.028	54.67×10^{-2}	8.16
0.9	16.2360	1250.0078×10^{-5}	0.43	1.72	0.3349	0.1488	0.1518	13.36×10^{-2}	48.56

n	α	frequency ξ_k	damping η_k	critical radii n/ξ_k	critical radii $n/\epsilon\xi_k$	Coriolis split in frequency (6.6)	$\lvert A_{nk}\rvert$	$\lvert B_{nk}\rvert$	coastal amplitude $\lvert A_{nk}\rvert$	max $\lvert B_n\rvert$ (4.9)
				$\epsilon = 0.50$						
3	0.0	5.6323	0.6323	0.53	1.07	0.1691	0.5166	0.5166	—	1.63
	0.1	5.6322	0.6321	0.53	1.07	0.1691	0.5166	0.5165	0.0155	1.63
	0.2	5.6274	0.6241	0.53	1.07	0.1673	0.5130	0.5087	0.1186	1.63
	0.3	5.5826	0.5660	0.54	1.07	0.1659	0.4812	0.4514	0.3439	1.60
	0.4	5.4265	0.4491	0.55	1.11	0.2187	0.3968	0.3435	0.5388	1.53
	0.5	5.2204	0.3858	0.58	1.15	0.3229	0.3394	0.3011	0.6266	1.56
	0.6	5.1110	0.4355	0.59	1.17	0.4339	0.3500	0.3608	0.7330	1.66
	0.7	5.1409	0.6604	0.58	1.17	0.5548	0.3862	0.5659	0.8987	1.71
	0.8	5.1416	1.1125	0.58	1.17	0.5664	0.2891	0.8753	0.8740	1.57
	0.9	4.9831	1.5673	0.60	1.20	0.4380	0.1497	1.156	0.6647	1.48
5	0.0	8.0208	0.2194	0.62	1.25	0.1046	0.2439	0.2439	—	2.22
	0.1	8.0208	0.2194	0.62	1.25	0.1046	0.2439	0.2439	0.0002	2.22
	0.2	8.0207	0.2193	0.62	1.25	0.1046	0.2438	0.2438	0.0049	2.22
	0.3	8.0170	0.2176	0.62	1.25	0.1051	0.2426	0.2422	0.0332	2.23
	0.4	7.9775	0.2012	0.63	1.25	0.1126	0.2308	0.2267	0.1133	2.25
	0.5	7.8217	0.1555	0.64	1.28	0.1561	0.1952	0.1858	0.2171	2.39
	0.6	7.5997	0.1255	0.66	1.32	0.2425	0.1742	0.1678	0.2836	2.67
	0.7	7.5575	0.1594	0.66	1.32	0.3374	0.2154	0.2235	0.3779	2.80
	0.8	7.9425	0.3799	0.63	1.26	0.4331	0.3410	0.4743	0.6061	2.50
	0.9	8.5729	1.2340	0.58	1.17	0.4307	0.2616	1.362	0.7609	2.21

TABLE 1 (*cont.*)

n	α	frequency ξ_k	damping η_k	critical radii n/ξ_k	critical radii $n/\epsilon\xi_k$	Coriolis split in frequency (6.6)	$\lvert A_{nk}\rvert$	$\lvert B_{nk}\rvert$	coastal amplitude $\lvert A_{nk}\rvert$	max $\lvert B_n\rvert$ (4.9)
				$\epsilon = 0.50$ (*cont.*)						
7	0.0	10.4438	0.7243×10^{-1}	0.67	1.34	0.0646	0.1427	0.1427	—	3.94
		13.8227	0.7745	0.51	1.01	0.1327	0.5376	0.5376	—	1.39
	0.1	10.4438	0.7243×10^{-1}	0.67	1.34	0.0646	0.1427	0.1427	0.0002×10^{-2}	3.94
		13.8227	0.7745	0.51	1.01	0.1327	0.5376	0.5376	0.0006×10^{-1}	1.39
	0.2	10.4438	0.7243×10^{-1}	0.67	1.34	0.0646	0.1427	0.1427	0.0270×10^{-2}	3.94
		13.8226	0.7745	0.51	1.01	0.1327	0.5376	0.5375	0.0663×10^{-1}	1.39
	0.3	10.4437	0.7239×10^{-1}	0.67	1.34	0.0646	0.1427	0.1427	0.3923×10^{-2}	3.94
		13.8179	0.7674	0.51	1.01	0.1317	0.5364	0.5319	0.8580×10^{-1}	1.39
	0.4	10.4356	0.7117×10^{-1}	0.67	1.34	0.0659	0.1410	0.1408	2.335×10^{-2}	3.96
		13.7045	0.6604	0.51	1.02	0.1343	0.4976	0.4435	0.3830	1.34
	0.5	10.3587	0.6126×10^{-1}	0.68	1.35	0.0825	0.1272	0.1261	7.468×10^{-2}	4.12
		13.3183	0.5530	0.53	1.05	0.2248	0.4154	0.3789	0.6223	1.37
	0.6	10.1122	0.4193×10^{-1}	0.69	1.38	0.1510	0.1007	0.0991	12.52×10^{-2}	4.73
		13.4217	0.9128	0.52	1.04	0.3363	0.4682	0.7323	0.8415	1.60
	0.7	9.9029	0.3922×10^{-1}	0.71	1.41	0.2520	0.1061	0.1059	16.64×10^{-2}	5.40
		13.9109	2.1188	0.50	1.01	0.3540	0.2346	1.773	0.7587	1.67
	0.8	10.2299	0.9556×10^{-1}	0.68	1.37	0.3526	0.2041	0.2180	29.84×10^{-2}	4.56
	0.9	11.6647	7.0216×10^{-1}	0.60	1.20	0.4231	0.3988	1.001	70.95×10^{-2}	2.85

Also, the sequences in the individual graphs of figure 7 clarify the effect that the island, 'growing' on the underlying sill, has on the individual modes. The profiles in the individual graphs of figure 7*a* plainly show not only that the amplitude of the mode decays rapidly towards the coast from the inner critical circle (of radius $\rho_k = n/\xi_k$) while the latter is on the shelf ($\alpha < \rho_k$), but also that the growing island has negligible effect on the mode while it is interior to the inner critical circle, verifying a conjecture of Longuet-Higgins (1967, § 9). Figure 5 and table 1 concur that ξ_k is little changed while $\alpha < \rho_k$. As α increases from zero, both ξ_k and η_k decrease slowly until

$$\alpha = n/\xi_k = \alpha_k, \quad \text{say}, \tag{3.20}$$

i.e. until the coast coincides with the mode's inner critical circle. At $\alpha = \alpha_k$, the mode takes its greatest amplitude at the coast (compared with unity at the edge). With further increasing α, the situation is as described in appendix A for the ledge wave-mode (A 2) with the width of the ledge decreasing; the components (3.3) and (3.2) of the motion on the shelf, reflected alternately from the coast and internally from the edge, have to turn in order that the phase change incurred in the crossing of the shelf compensates for the decreasing width of the latter. The frequency ξ_k increases, and the angle of incidence at the edge $\phi_i = \arcsin n/\xi_k$, decreases towards the critical angle $\phi_c = \arcsin \epsilon$ (appendix A). At the same time the damping factor η_k increases; the mode leaks energy to the ocean at a greater rate. The plots in figure 7 (*a*) show that the amplitude at the coast decreases, the nodal circles (if any) move towards the edge, and the exponential decay in amplitude in the ocean becomes less noticeable. Finally, as the α-curve passes through the region about the line (3.15), i.e. as ϕ_i decreases through ϕ_c, η_k increases rapidly, and the profile (figure 7*b*) changes from that of an *almost trapped* wave motion to that of a 'leaky wave' (appendix A); the profile is 'wave-like' in the ocean, even near the edge. Indeed, one can roughly calculate

the value of α at which the transition occurs; the cutoff shelf width for the mode [cf. appendix A] is equal to $1-\beta_k$, where β_k is defined in (A 13). In other words, we have set (cf. (3.17) and (A 14))

$$\alpha = 1-\beta, \tag{3.21}$$

which equates the long-wave speeds across the shallow-water regions (normal to the coast) of the models defined, respectively, by (2.1) and (A 1). As might be expected, the formula is most accurate when n is large, with k and ϵ small, i.e. when the influence of the curvature of the shelf is least.

The description can be extended to the higher order modes, i.e. to the modes represented by the ν_k emanating from the *first-system* roots of $E(\nu;\ 0.25, 0, 5)$ to the right of the line (3.15). Clearly, these modes are 'leaky waves' for all α.

Thus, we see that, for the particular island-shelf systems under consideration ($\epsilon = 0.25$), there exists an infinite number of 'trapped-leaky' wave-modes at each n. The modes with frequencies significantly less than n/ϵ are *almost trapped* on the shelf; these modes can be determined, roughly, from the simpler model (A 1) by way of (3.21). In addition, there exists a much smaller set of free wave motions represented by the eigenfrequencies on the α-curves attached to the *second-system* roots of $E(\nu;\ \epsilon, 0, n)$ correlated with the values ϵ_{nl}, where $l \geqslant 1$. It is obvious that these modes are generated in the ocean about the 'shelf-island' of radius a_2; they are heavily damped, and have negligible amplitude over the shelf. We now verify that the conclusions concerning the nature of the free wave-modes (3.1) are valid for all ϵ in the range (3.9).

It has been shown by Longuet-Higgins (1967, § 6) that quite accurate values of the frequencies of the modes, *almost trapped* over the circular sill, can be obtained without evaluating

$$E(\nu;\ 0.25, 0, n).$$

An extension of the argument to the oscillations of the model with $\alpha \neq 0$ (Summerfield 1969) again yields accurate estimates of the frequencies of the *almost trapped* modes. The success of the argument not only clearly demonstrates the waveguide nature of the shelf, but also reveals, that the frequencies are only weakly dependent on ϵ. It follows that, when $\epsilon < 0.25$, any 'trapped-leaky' mode will be more effectively trapped on the shelf than the corresponding mode at $\epsilon = 0.25$ with the same n, α and k, for the angle of incidence (3.4) at the edge will exceed the critical angle by a greater amount than at $\epsilon = 0.25$. The corresponding damping factor will be smaller, so that the eigenfrequency will be displaced towards the real axis, virtually along a line parallel to the imaginary axis. On the other hand, when $\epsilon > 0.25$, the leakage will be greater, and the displacement will be away from the real axis. Figure 5 demonstrates this for $\epsilon = 0.50$; all the α-curves of the roots of $E(\nu;\ \epsilon = 0.50, \alpha, n)$, corresponding to the modes represented at $\epsilon = 0.25$, have been plotted. A careful examination of the subfigures again reveals the 'filling-in' role in the 'trapped-leaky' mode α-curve pattern played by the α-curve started on the *second-system* root of $E(\nu;\ 0.50, 0, n)$ nearest to ϵ_{n0}. The fewer number of *almost trapped* modes is emphasized by the smaller number of eigenfrequencies recorded in table 1. The α-curves of the eigenfrequencies representing 'shelf-island' modes confirm that these modes are little affected by the depth of water on the shelf.

Figure 5 also plots the α-curves of the roots of $E(\nu;\ \epsilon = 0.75, \alpha, n)$, corresponding to the modes represented at $\epsilon = 0.25$; those zeros representing 'trapped-leaky' modes are even farther from the real axis than the corresponding values at $\epsilon = 0.25$ and $\epsilon = 0.50$. A close inspection of these graphs reveals that a subtle change has taken place in the α-curve pattern. At all n, the α-curve

started on the *second-system* root of $E(\nu; 0.75, 0, n)$ nearest to ϵ_{n0}, ends on ϵ_{n0}, while, for all $k \geqslant 0$, the ν_k asymptote to the values (3.17) where $j = k+1$, as α approaches 1. The fundamental mode is represented by the first-mentioned α-curve at large n. It can be argued that this change in α-curve pattern occurs when $\epsilon > 2/\pi$, on the assumption that the pattern at smaller ϵ is due to *first-system* roots of $E(\nu; \epsilon, 0, n)$ being to the left of the line (3.15) (Summerfield 1969).

On the other hand, the change in the α-curve pattern when $\epsilon > 2/\pi$ allows one to predict what happens when ϵ approaches 1, i.e. when the ocean rises, leaving in the limit ($\epsilon = 1$), a vertical-walled island of radius $a_1 (= \alpha)$ in an ocean of uniform depth h_1. Numerical computation verifies that the α-curves attached to the *second-system* roots of $E(\nu; \epsilon, 0, n)$ aline themselves along the curves $\nu = \mu_{n1}/\alpha$, whereas the ν_k defined in (3.18) go to infinity, along straight lines parallel to the imaginary axis. In other words, the only finite-valued roots of $E(\nu; \epsilon = 1, \alpha \neq 0, n)$ and $E(\nu; \epsilon \neq 1, \alpha = 1, n)$ are the zeros of, respectively, $H_n^{(1)\prime}(\alpha\nu)$ and $H_n^{(1)\prime}(\epsilon\nu)$. Thus, at each n, there exists a finite number of heavily damped modes for a cylindrical island standing in an ocean of uniform depth.

By the use of the step-by-step method of computation, one can also show that the one-to-one correspondence between roots of $E(\nu; \epsilon, 0, n)$ and those of $H_n^{(1)\prime}(\epsilon\nu)$ carries over onto the sheet $-\frac{5}{2}\pi < \arg\nu < -\frac{1}{2}\pi$ of the Riemann surface (Summerfield 1969). The represented motions will not be considered here.

Finally, we note that the zeros of $H_n^{(1)\prime}(\epsilon\nu)$ are roots of E only when $\alpha = 1$. In addition, the zeros of $H_n^{(1)}(\epsilon\nu)$ are never roots of E (Summerfield 1969), i.e. the modes (3.1) never have nodal circles coincident with the edge. Hence, there is both mass and momentum transport across the edge in every mode. Also, the non-vanishing of both $H_n^{(1)\prime}(\epsilon\nu)$ and $H_n^{(1)}(\epsilon\nu)$ when $\alpha < 1$ implies that neither square-bracketed term in (3.5) is zero; it follows that the form (3.1) of the free mode expression is valid throughout.

4. Response at the coast to monochromatic radiation from the ocean

In this section, we investigate the response of the island's near-shore waters to a sinusoidal train of plane waves incident on the edge from the ocean. Without loss of generality, the direction of propagation of the oceanic waves may be taken along $\theta = 0$, i.e. to the right along the x-axis (figure 1).

Provided σ and k_2 are real, and are related as in (2.6) the expression

$$\zeta_\infty = \exp\{\mathrm{i}(k_2 r\cos\theta - \sigma t)\}, \tag{4.1}$$

represents a simple harmonic train of long waves propagating through the ocean of the island-shelf model (2.1). When these waves encounter the shelf one expects them to be partly converted into motions over the shelf, and partly scattered to infinity in the ocean. At large distances from the island it is assumed that $\zeta \sim \zeta_\infty$.

Since ζ_∞ can be written

$$\zeta_\infty = \sum_{n=-\infty}^{\infty} \tfrac{1}{2}\mathrm{i}^n [H_n^{(1)}(k_2 r) + H_n^{(2)}(k_2 r)] \exp\{\mathrm{i}(n\theta - \sigma t)\} \quad (r \neq 0), \tag{4.2}$$

one assumes that the solution for its interaction with the island-shelf topography has the form

$$\zeta(r,\theta,t) = \sum_{n=-\infty}^{\infty} \exp\{\mathrm{i}(n\theta - \sigma t)\} \begin{cases} A_n H_n^{(1)}(k_1 r) + B_n H_n^{(2)}(k_1 r) & (0 < a_1 < r < a_2), \\ (C_n + \tfrac{1}{2}\mathrm{i}^n) H_n^{(1)}(k_2 r) + \tfrac{1}{2}\mathrm{i}^n H_n^{(2)}(k_2 r) & (r > a_2), \end{cases} \tag{4.3}$$

where the terms with the coefficients A_n and B_n represent the excited shelf motions, those with C_n, the energy scattered to infinity in the horizontal plane. The coefficients are uniquely determined by the boundary conditions (2.8), (2.9) and (2.10); one can readily verify that

$$A_n = \frac{2\mathrm{i}^{n+1}H_n^{(2)\prime}(\alpha\nu)}{\pi\epsilon\nu E(\nu;\,\epsilon,\,\alpha,\,n)}, \quad B_n = \frac{-2\mathrm{i}^{n+1}H_n^{(1)\prime}(\alpha\nu)}{\pi\epsilon\nu E(\nu;\,\epsilon,\,\alpha,\,n)}, \tag{4.4}$$

$$C_n + \tfrac{1}{2}\mathrm{i}^n = (-1)\,\tfrac{1}{2}\mathrm{i}^n \frac{E_s(\nu;\,\epsilon,\,\alpha,\,n)}{E(\nu;\,\epsilon,\,\alpha,\,n)}, \tag{4.5}$$

where $\nu, \epsilon, \alpha(\neq 0)$ and E are as defined in (3.8), (3.9), (3.10) and (3.12), and $E_s(\nu;\,\epsilon,\,\alpha,\,n)$ has the same form as E but with $H_n^{(1)}(\epsilon\nu)$ and $H_n^{(1)\prime}(\epsilon\nu)$, respectively, replaced by $H_n^{(2)}(\epsilon\nu)$ and $H_n^{(2)\prime}(\epsilon\nu)$. With these coefficients, (4.3) yields the formal solution of the problem. We note that the corresponding solution for the model where there is no island on the underlying sill ($\alpha = 0$), can be obtained from (4.3) by taking the appropriate limit (cf. § 3); the coefficients can also be determined separately from (4.4) and (4.5).

The moduli of A_n, B_n and C_n represent the amplitudes of, respectively, the waves on the shelf propagated towards the edge, the shelf-waves propagated towards the coast and the waves scattered in the ocean, in response to the periodic incident wave of unit amplitude. Since σ is real, it follows from (4.4) that

$$|A_n| = |B_n|; \tag{4.6}$$

similarly, $|C_n + \tfrac{1}{2}\mathrm{i}^n| = \tfrac{1}{2}$. Thus, both on the shelf and in the ocean, the waves propagated towards and away from the island have equal energy. The motions scattered in the ocean will be of no further interest in the present context.

The disturbance in water level at the coast is found by setting $r = a_1(>0)$ in the appropriate part of (4.3); it is (the real part of)

$$\zeta(a_1, \theta, t) = \sum_{n=-\infty}^{\infty} \exp\{\mathrm{i}(n\theta - \sigma t)\} \frac{8i^n}{\pi^2\epsilon\alpha\nu^2 E(\nu;\,\epsilon,\,\alpha,\,n)}, \tag{4.7}$$

where ϵ and α are the constants determined by the dimensions of the island-shelf complex, and ν is the non-dimensional frequency of the incident waves. Upon noting that

$$E(\nu;\,\epsilon,\,\alpha+0,\,-n) = (-1)^n E(\nu;\,\epsilon,\,\alpha,\,n),$$

one can simpify the expression to

$$\zeta(a_1, \theta, t) = \frac{8}{\pi^2\epsilon\alpha\nu^2} \exp\{-\mathrm{i}\sigma t\}\left\{\frac{1}{E(\nu;\,\epsilon,\,\alpha,\,0)} + 2\sum_{n=1}^{\infty} \frac{\mathrm{i}^n \cos n\theta}{E(\nu;\,\epsilon,\,\alpha,\,n)}\right\}, \tag{4.8}$$

which form reveals the excitation along the coast to be symmetric with respect to the normal to the incident waves which passes through the centre of the island, as one would expect. Also, at every location, the perturbed surface oscillates with the same frequency as the incident waves. Furthermore, the response is composed of a sum of standing waves of azimuthal dependences $\cos n\theta$, with amplitudes proportional to $|E(\nu;\,\epsilon,\,\alpha,\,n)|^{-1}$. If one of the latter happens to be much greater than all the others, the coastline response will be dominated by the corresponding cosine term. It follows that points on the coast may exist where there is virtually no movement in the water's surface; intermediate spots will suffer relatively large-amplitude oscillations. In order to discern the nature of the dependence of the $|E(\nu;\,\epsilon,\,\alpha,\,n)|^{-1}$ on the various parameters (including ν), and hence that of $\zeta(a_1, \theta, t)$, it is first necessary to investigate the coefficients (4.4).

Figure 8 shows representative plots of $|B_n|$ as a function of ν (n, ϵ and α held fixed). One observes that $|B_n|$ increases sharply whenever the frequency of the incident waves is near that of an *almost trapped* mode (3.1) of the same along-edge wavenumber n, i.e. when ν is in the neighbourhood of a root of $E(\nu; \epsilon, \alpha, n)$ very near the real axis. On expanding E in a Taylor series about such a zero, ν_k [defined in (3.18)], ($\eta_k \ll 1$) it is easily argued that the peak value of the response occurs when $\nu \doteqdot \xi_k$, and that

$$\max |B_n| \doteqdot \frac{2}{\pi\epsilon\eta_k} \frac{|H_n^{(1)\prime}(\alpha\nu_k)|}{|\nu_k E'(\nu_k; \epsilon, \alpha, n)|}; \tag{4.9}$$

furthermore, $|B_n|$ exceeds half the peak value whenever

$$|\nu - \xi_k| < \sqrt{3}\eta_k. \tag{4.10}$$

With the aid of these formulae, one can deduce the dependences on the various parameters n, ϵ and α of the significant features of the local maxima in $|B_n|$ from the α-curve computations of the previous section.

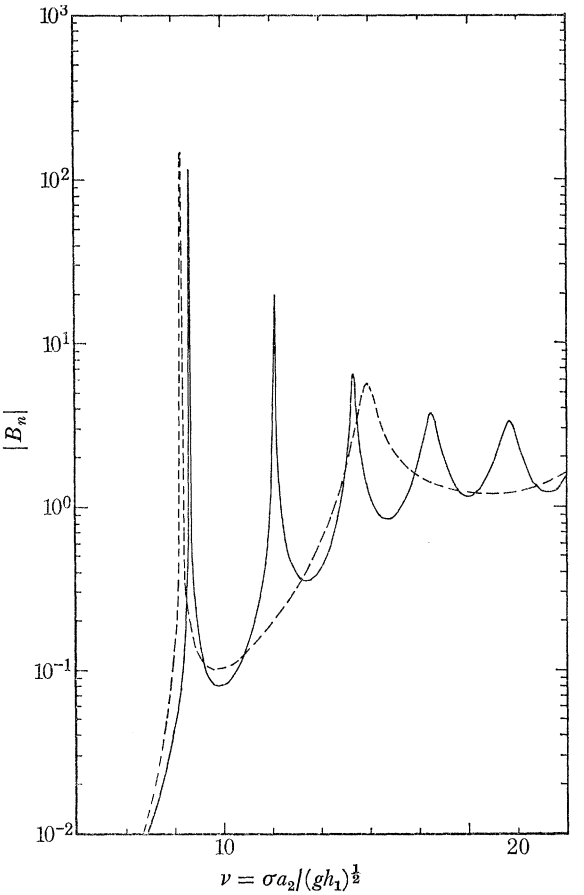

FIGURE 8. Graphs of $|B_n|$ for $n = 5$, $\epsilon = 0.25$, $\alpha = 0.2$ (full curve) and $\alpha = 0.7$ (broken curve), giving the amplitude of the response as a function of the frequency ν of the incident waves.

Consider, for example, the magnitude of a local maximum, i.e. max $|B_n|$. Figure 9*a* graphs against α the values (4.9) associated with the zeros ν_0, ν_1 and ν_2 of $E(\nu; 0.25, \alpha, 7)$ (n, ϵ and mode-order k held fixed); as expected, max $|B_n|$ increases as the damping factor, η_k, of the corresponding *almost trapped* mode (figure 5*h*; table 1) decreases. In particular, the greatest max $|B_n|$ occurs when (3.20) is satisfied (the dotted point on each curve); then max $|B_n|$ decreases rapidly

as α increases towards the cut-off shelf width of the corresponding mode. The plots of figure 9*b* and the values in table 1 reveal that max $|B_n|$ grows with increasing n (ϵ, α and k held fixed); the rate of increase is extremely rapid at small $\epsilon(=0.25)$, much slower at larger $\epsilon=(0.50)$, mirroring the rate of decrease in the damping factors, η_k, of the corresponding *almost trapped* modes (3.1). These examples show, not only how large are the amplitudes that can be built up over the shelf by the trapping effect of the bottom topography about the island (as has already been pointed out by Longuet-Higgins 1967, § 7)], but also that their magnitudes depend strongly on the rate of energy loss to the ocean of the corresponding *almost trapped* modes which, in turn, are related to the angles of incidence at the edge of the modes' shelf-components. Indeed, table 1 verifies that there is qualitative agreement between the max $|B_n|$ and the amounts by which these angles exceed the critical angle ϕ_c, i.e. between max $|B_n|$ and, say, the quantities $n/\xi_k-\epsilon$.

The error involved in taking the estimate (4.9) as the peak value of the local maximum (in the graph of $|B_n|$ against ν) can also be inferred from the numbers in table 1. The quantity (4.9) equals $|B_{nk}|/(\epsilon\eta_k)$ where $|B_{nk}|$ is defined in (5.9). Further, the same relationship holds between

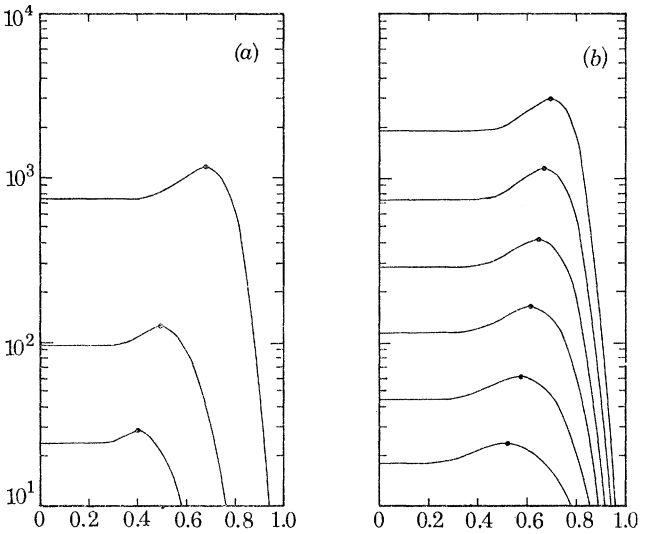

FIGURE 9. Graphs of max $|B_n|$, (4.9), as a function of α: (*a*) the local maxima corresponding to the roots ν_0 (top), ν_1 (middle) and ν_2 (bottom) of $E(\nu; 0.25, \alpha, 7)$; (*b*) the local maxima corresponding to the zero ν_0 of $E(\nu; 0.25, \alpha, n=3(1)8)$.

the similar approximation to max $|A_n|$, and $|A_{nk}|$. But (4.6) is an identity for all ϵ, α, n and real $\nu(\neq 0)$. Hence, it follows that the difference between $|B_{nk}|$ and $|A_{nk}|$ is an indication of the magnitude of the error between the peak value of $|B_n|$ and the estimate given by (4.9). The $|A_{nk}|$ and $|B_{nk}|$ recorded in table 1 confirm that the error is relatively small while $\eta_k \ll 1$. Further computation of $|B_n|$, as a function of ν, over various n, ϵ and α, verifies that (4.10) yields an adequate description of the width of the local maximum in the neighbourhood of $\nu=\xi_k$ under the same condition (Summerfield 1969).

One can now resolve the circumstances under which the water level at the island's coastline experiences large oscillations. First, the frequency of the incident waves must satisfy (4.10) where ξ_k is the frequency of one of the island-shelf system's *almost trapped* modes of oscillation. Then the amplitude response function of the same order n is large; it dominates the set of all amplitude response functions because the interval specified in (4.10), being small, excludes the similar

ranges of all other *almost trapped* modes. Secondly, in order that $|E(\nu;\epsilon,\alpha,n)|^{-1}$ be large too, one requires

$$\alpha > \alpha_k - \delta_k, \tag{4.11}$$

where α_k is defined in (3.20) and $\delta_k(>0)$ is a small number to be determined. While $\alpha < \alpha_k$, the free mode's inner critical circle (a wave caustic) is on the shelf (§ 3), and the exponential decrease in the wave amplitude from there towards the coast reduces the amplitude of the forced waves as seen at the latter boundary. On the other hand, when $\alpha > \alpha_k$, it is primarily the diminution in $\max|B_n|$ which decreases the amplitude of the forced waves; the dependence of the maximum of the radial component of (3.1) (figure 7) on the parameters n, ϵ and α is much weaker than for $\max|B_n|$. With (4.10) and (4.11) both satisfied, the expression (4.8) is dominated by the $\cos n\theta$ term; figure 10(*a*) demonstrates how large the fluctuations in the coastline water level can be (at antinodes) under these conditions. Figure 10*b* shows what happens when (4.10) is satisfied,

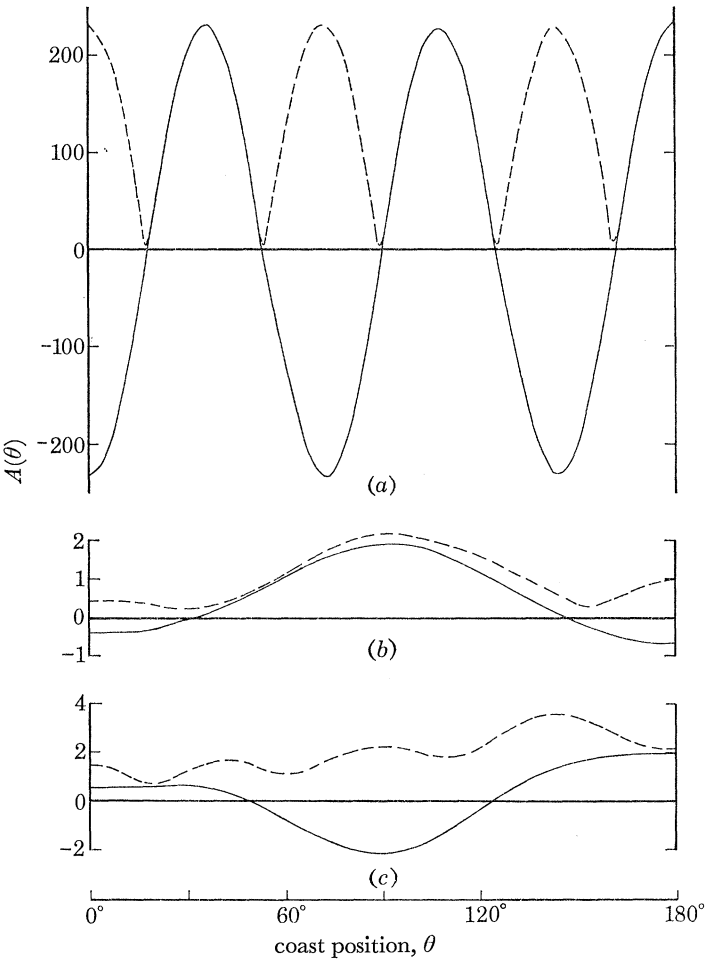

FIGURE 10. Relative amplitude versus azimuth for three response patterns (4.8) at the coast. With the real part of (4.8) written as $A(\theta)\cos[\sigma t+\delta(\theta)]$, the solid lines represent $A(\theta)\cos\delta(\theta)$ and the broken lines, $A(\theta)$; note that $\theta = 0°$ is in the lee of the island. Note also the different vertical scales. (*a*) $\alpha = 0.7$, $\epsilon = 0.25$, $\nu = 8.3013374$ (table 1, $n = 5$); (*b*) $\alpha = 0.4$, $\epsilon = 0.25$, $\nu = 8.5555946$; (*c*) $\alpha = 0.7$, $\epsilon = 0.25$, $\nu = 8.2$.

but not (4.11); it follows that, for any particular mode, the value of δ_k required in (4.11) can be calculated by numerical computation of $|E(\nu;\epsilon,\alpha,n)|$ over a range of α with upper limit specified by (3.20). Finally, figure 10*c* exemplifies the case where (4.10) is not valid (and also the situation where η_k is too large).

5. The response at the coast to a travelling pulse

We have seen how large amplitude oscillations may be observed at the coast, due to the incidence of simple-harmonic plane-wave radiation on the edge from the ocean. Here, we examine the disturbance at the coast resulting from the model's encounter with a line-pulse of energy sweeping across the ocean.

Once it has been noticed that a straight line-pulse propagated across the ocean in the positive x direction (along $\theta = 0$ in figure 1) may be represented by

$$\sigma_2^{-1}\delta(t - x(gh_2)^{-\frac{1}{2}}) = \frac{1}{2\pi\sigma_2}\int_C \exp\{\mathrm{i}(k_2 x - \sigma t)\}\,\mathrm{d}\sigma, \tag{5.1}$$

where $\delta(t)$ is the Dirac delta function, $x = r\cos\theta$ (figure 1), k_2 is defined in (2.6), C is the contour shown in figure 11, and where $\sigma_2 = (gh_2)^{\frac{1}{2}}/a_2$ has been introduced for convenience, the formal solution for the motions excited on the shelf by the incidence of the pulse (5.1) on the edge follows rapidly from (4.3). The disturbance on the shelf is given by

$$\zeta(r, \theta, t) = \sum_{n=-\infty}^{\infty} P_n(r, t)\exp\{\mathrm{i}n\theta\} \quad (0 < a_1 < r < a_2), \tag{5.2}$$

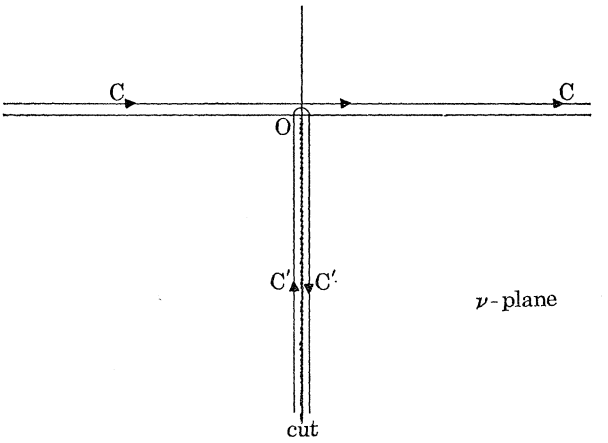

Figure 11. A sketch of the contours C and C'.

where, in terms of the dimensionless quantities of § 3,

$$P_n(r, t) = \frac{\mathrm{i}^{n+1}}{\pi^2}\int_C \frac{H_n^{(2)\prime}(\alpha\nu)\,H_n^{(1)}(\nu r/a_2) - H_n^{(1)\prime}(\alpha\nu)\,H_n^{(2)}(\nu r/a_2)}{\nu E(\nu;\,\epsilon,\,\alpha,\,n)}\exp\{-\mathrm{i}\nu\bar{t}\}\,\mathrm{d}\nu, \tag{5.3}$$

and

$$\bar{t} = t(gh_1)^{\frac{1}{2}}/a. \tag{5.4}$$

Now, the integrand of $P_n(r, t)$ is regular everywhere except for a logarithmic singularity at the origin and simple poles at the zeros of $E(\nu;\,\epsilon,\,\alpha,\,n)$, all of which lie below the real axis. By deforming C into infinite semicircles, respectively, in the upper and lower half planes, one can readily verify that

$$P_n(r, \bar{t} < -1) = 0, \tag{5.5}$$

and

$$P_n(r, \bar{t} > 1) = -2\pi\mathrm{i}\sum_l^{\text{residue of integrand of (5.3) at the zero } \nu_l \text{ of } E} + R_n(r, t), \tag{5.6}$$

where

$$R_n(r, t) = \frac{\mathrm{i}^{n+1}}{\pi^2}\int_{C'} \frac{H_n^{(2)\prime}(\alpha\nu)\,H_n^{(1)}(\nu r/a_2) - H_n^{(1)\prime}(\alpha\nu)\,H_n^{(2)}(\nu r/a_2)}{\nu E(\nu;\,\epsilon,\,\alpha,\,n)}\exp\{-\mathrm{i}\nu\bar{t}\}\,\mathrm{d}\nu, \tag{5.7}$$

and the summation with respect to l extends over all the zeros of E on the sheet $-\frac{1}{2}\pi < \arg\nu < \frac{3}{2}\pi$ of the Riemann surface, including both *first-* and *second-system* roots and their reflexions in the imaginary axis, which is cut along its negative section (§ 3). The contour C' runs up the left-hand side of the cut (from $-\mathrm{i}\infty$ to 0 with $\arg\nu \doteqdot \frac{3}{2}\pi$) and down the right-hand side (from 0 to $-\mathrm{i}\infty$ with $\arg\nu \doteqdot -\frac{1}{2}\pi$); it excludes the singularity of E at the origin from the summation. On evaluating the residue at $\nu = \nu_l$, one finds that

$$P_n(r, \bar{t} > 1) = \sum_l \{A_{nl} H_n^{(1)}(\nu_l r/a_2) - B_{nl} H_n^{(2)}(\nu_l r/a_2)\} \exp\{-\mathrm{i}\nu_l \bar{t}\} + R_n(r, t), \tag{5.8}$$

where

$$A_{nl} = \frac{2\mathrm{i}^n}{\pi} \frac{H_n^{(2)'}(\alpha\nu_l)}{\nu_l E'(\nu_l; \epsilon, \alpha, n)}, \quad B_{nl} = A_{nl} \frac{H_n^{(1)'}(\alpha\nu_l)}{H_n^{(2)'}(\alpha\nu_l)}. \tag{5.9}$$

Substitution from (5.8) backs into (5.2) discloses the response of the shelf to the impulse as a sum of the free modes (3.1), each decaying exponentially in time, and a sum of transient 'tails', represented by the R_n.

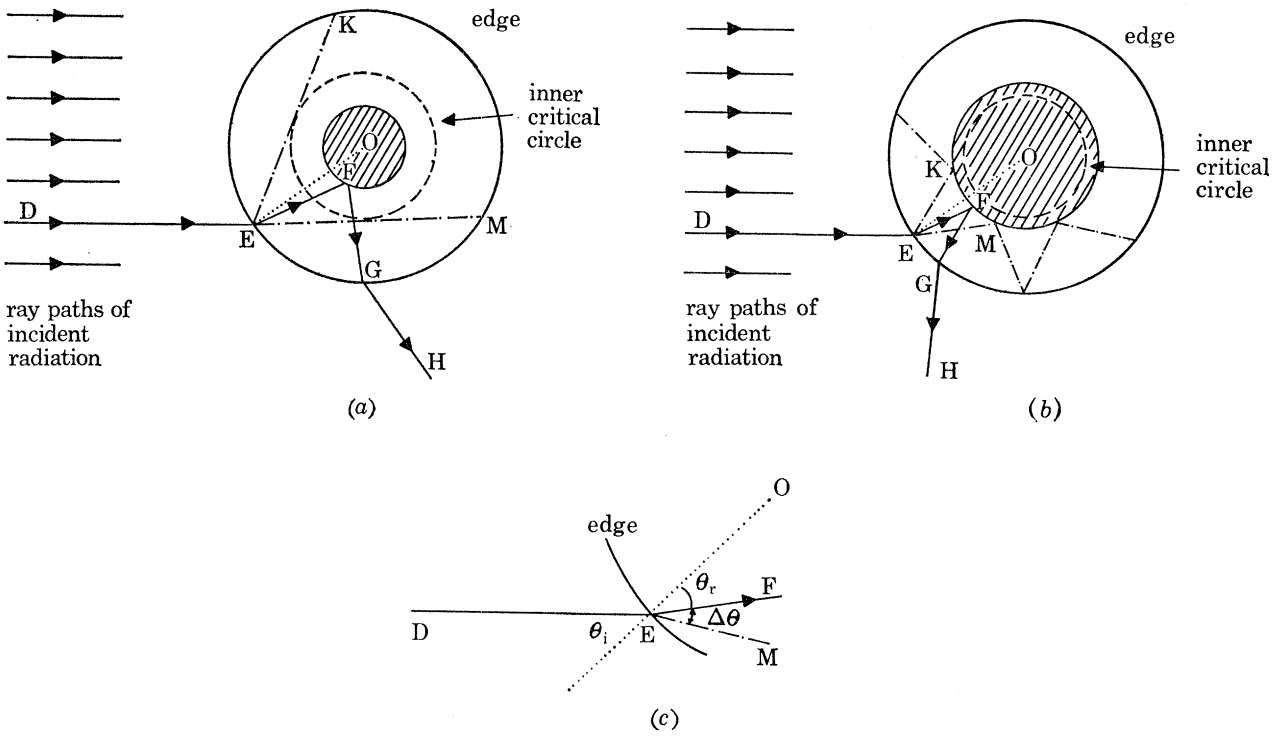

FIGURE 12. Plan view of the path of the ray DEFGH of the line-pulse (5.1) which meets the edge of the island-shelf system (centre O) at E. The broken circle describes the inner critical circle of an *almost trapped* mode, and the dash-dotted lines are representative wave rays. (*a*) The island is interior to the mode's inner critical circle ($\alpha < \alpha_k$); (*b*) the shelf-components of the mode are reflected from the coast ($\alpha > \alpha_k$, but $\xi_k < n/\epsilon$); (*c*) the angle of refraction at E of the ray of the pulse, $\theta_r \doteqdot \arcsin(\epsilon \sin\theta_i)$ is always less than the angle OEM $= \phi_i$, (3.4), for every *almost trapped* mode.

The formal solution for the motions scattered in the ocean as a result of the encounter between the pulse and the island-shelf complex can be derived from (4.3) in a similar manner. Although the scattered waves will not be examined here, some consideration has been given to them by Summerfield (1969).

The amplitude of each excited mode (3.1) is virtually given by the appropriate $|B_{nl}|$. Table 1

tabulates the values of $|B_{nk}|$, and $|A_{nk}|$,† for the *almost trapped* modes represented there. We show that these amplitudes are qualitatively consistent with a ray-theory argument for the generation of the modes by the pulse.

Each ray path of the pulse which meets the edge (figure 12) necessarily intersects rays of every *almost trapped* mode on the shelf. The angle of intersection between one such ray DEFGH of the pulse, and the rays of one particular *almost trapped* mode, is a minimum, $\Delta\theta$, for that ray EM of the mode which also meets the edge at E. Summed over every ray path of the pulse which meets the edge, one expects this situation to correspond to the most efficient generation of the mode by the radiation from the ocean. Consequently, the influence which the parameters n, ϵ and α (as well as the mode-order k) exert in the excitation of the mode can be determined from their effect on $\Delta\theta$; the smaller (larger) $\Delta\theta$, the larger (smaller) the magnitude of $|B_{nk}|$. Figure 12*c* shows that

$$\Delta\theta = \arcsin(n/\xi_k) - \theta_r, \tag{5.10}$$

where θ_r is the angle of refraction of the ray DEFGH at the edge; it is a function of ϵ only. The values in table 1 verify that while three of n, ϵ, α and k are held fixed, and the fourth varied over its range, the magnitude of $|B_{nk}|$ changes in the expected manner.

The disturbance in water level at the coast is found either by setting $r = a_1$ in (5.2), or by direct integration of (4.7). With the symmetry in the zeros of E about the imaginary axis taken into account, the appropriate expression is

$$\zeta(a_1, \theta, \bar{t} > 1) = \sum_{n=0}^{\infty} \gamma_n \cos n\theta \{\sum_{l^*} -\mathrm{i}^{n+1} \exp\{-\eta_{l^*}\bar{t}\} \mathscr{R}(\Lambda_{nl^*} \exp\{-\mathrm{i}\xi_{l^*}\bar{t}\}) + R_n(a_1, t)\}, \tag{5.11}$$

where $\gamma_0 = 1$ and $\gamma_n = 2$ when $n \neq 0$. The summation with respect to l^* extends only over all the *first-* and *second-system* roots of $E(\nu; \epsilon, \alpha, n)$ in the fourth quadrant, and

$$\Lambda_{nl^*} = \frac{16}{\pi^2 \alpha \nu_{l^*}^2 E'(\nu_{l^*}; \epsilon, \alpha, n)}. \tag{5.12}$$

Again, the excitation along the coast is symmetric with respect to the normal to the line-pulse which passes through the centre of the island; the standing wave configuration results from identical motions being propagated in opposite directions along the shelf. The initial amplitude of each mode (3.1) at the coast is given by the appropriate $|\Lambda_{nl^*}|$; the $|\Lambda_{nl^*}|$ recorded in table 1 show that, at best, the amplitude is comparable with the corresponding $|B_{nl^*}|$. But, at any time $\bar{t}(>0)$, the amplitude of the mode is also proportional to $\exp\{-\eta_{l^*}\bar{t}\}$, where η_l^* is its rate of damping. Thus, sometime after the passage of the pulse, the *almost trapped* modes of oscillation will dominate the contribution to the expression for $\zeta(a_1, \theta, \bar{t})$ from the free waves (3.1). In order to determine whether they also dominate the disturbance in water level at the coast it is necessary to evaluate the $R_n(a_1, t)$ for large $\bar{t}$.

It follows from (5.7), that

$$R_n(a_1, t) = \frac{4\mathrm{i}^n}{\pi^3 \alpha} \int_{C'} \frac{\exp\{-\mathrm{i}\nu\bar{t}\}\,\mathrm{d}\nu}{\nu^2 E(\nu; \epsilon, \alpha, n)}, \tag{5.13}$$

which can be evaluated asymptotically for large $\bar{t}$ by use of Watson's lemma. Near $\nu = 0$, one has

$$\nu^2 E(\nu; \epsilon, \alpha, n) = P \pm Q, \tag{5.14}$$

† If the motions (3.1) were perfectly trapped on the shelf, then $|A_{nk}| = |B_{nk}|$. The values show that $|A_{nk}| \approx |B_{nk}|$ while $\eta_k \ll 1$, but that $|A_{nk}| < |B_{nk}|$ when η_k is larger, as one might expect.

where
$$\left.\begin{aligned} P &\sim \begin{cases} 2^3\pi^{-2}\epsilon^{-1}\alpha^{-1} & (n=0), \\ 2^{n+1}n!\,\pi^2\epsilon^{-n-1}\alpha^{-n-1}\{1+\alpha^{2n}+\epsilon^2(1-\alpha^{2n})\}\nu^{-n} & (n>0), \end{cases} \\ Q &\sim \begin{cases} \mathrm{i}2^2\pi^{-1}\epsilon\alpha\nu^2 & (n=0), \\ -\mathrm{i}2^{-n+2}\pi^{-1}\epsilon^{n-1}\alpha^{-n-1}\{1+\alpha^{2n}-\epsilon^2(1-\alpha^{2n})\}\nu^n/(n-1)! & (n>0), \end{cases} \end{aligned}\right\} \tag{5.15}$$

and the positive or negative sign is to be taken according as ν lies to the right or left of the negative imaginary axis. Then, as $\bar{t}\to\infty$

$$\left.\begin{aligned} R_n(a_1,t) &\sim \frac{4\mathrm{i}^n}{\pi^3\alpha}\int_0^{-\mathrm{i}\infty}\frac{-2Q}{P^2}\exp\{-\mathrm{i}\nu\bar{t}\}\,\mathrm{d}\nu, \\ &= \begin{cases} \epsilon^3\alpha^2\bar{t}^{-3} & (n=0), \\ 8\dfrac{(3n)!}{(n!)^2(n-1)!}\left(\dfrac{-\epsilon}{2}\right)^{3n}\dfrac{1+\alpha^{2n}-\epsilon^2(1-\alpha^{2n})}{[1+\alpha^{2n}+\epsilon^2(1-\alpha^{2n})]^2}\dfrac{\alpha^n}{\bar{t}^{3n+1}} & (n>0). \end{cases} \end{aligned}\right\} \tag{5.16}$$

Thus, the contribution to (5.11) from the transient 'tails' is dominated by $R_0(a_1,t)$ when $\bar{t}$ is large. The following example shows that even $R_0(a_1,t)$ is much smaller in magnitude than the amplitudes of the slowly decaying *almost trapped* modes for moderately large $\bar{t}$.

TABLE 2. THE AMPLITUDES OF THE 'TRAPPED-LEAKY' MODES AND TRANSIENT TAILS AT THE COAST FOR $\bar{t}=10,\ 30;\ \alpha=0.7,\ \epsilon=0.25$

				$\bar{t}=10$		$\bar{t}=30$	
n	ξ_k	η_k	$\lvert A_{nk}\rvert$	$\lvert A\rvert\exp\{-\eta\bar{t}\}$	$\lvert R_n\rvert$	$\lvert A\rvert\exp\{-\eta\bar{t}\}$	$\lvert R_n\rvert$
0	5.37	-0.71	1.07	8.8×10^{-4}	—	5.6×10^{-10}	—
	15.74	-0.83	0.66	1.6×10^{-4}	7.7×10^{-6}	—	2.8×10^{-7}
	26.20	-0.84	0.52	1.2×10^{-4}	—	—	—
1	5.34	-0.75	1.25	6.9×10^{-4}	—	2.1×10^{-10}	—
	15.78	-0.85	0.68	1.4×10^{-4}	1.0×10^{-6}	—	1.3×10^{-8}
	26.23	-0.85	0.52	1.0×10^{-4}	—	—	—
2	5.52	-0.24	0.66	6.0×10^{-2}	—	4.9×10^{-4}	—
	15.88	-0.93	0.72	6.4×10^{-5}	5.2×10^{-11}	—	2.4×10^{-14}
	26.30	-0.88	0.53	8.0×10^{-5}	—	—	—
3	6.40	-0.31×10^{-1}	0.21	1.5×10^{-1}	—	8.4×10^{-2}	—
	15.97	-1.09	0.84	1.5×10^{-5}	2.3×10^{-15}	—	3.8×10^{-20}
	26.42	-0.93	0.55	5.0×10^{-5}	—	—	—
4	7.33	-0.33×10^{-2}	0.66×10^{-1}	6.4×10^{-2}	—	6.0×10^{-2}	—
	15.57	-1.22	1.29	6.4×10^{-6}	9.1×10^{-20}	—	5.7×10^{-26}
	26·58	-1.02	0·58	2.1×10^{-5}	—	—	—
5	8.30	-0.35×10^{-3}	$0{\cdot}20\times10^{-1}$	2.0×10^{-2}	—	2.0×10^{-2}	—
	15.87	-0.34	0.49	1.6×10^{-2}	3.5×10^{-24}	1.8×10^{-5}	8.2×10^{-32}
	26.74	-1.17	0.65	5.3×10^{-6}	—	—	—

Consider the particular island-shelf model where $\epsilon=0.25$ and $\alpha=0.7$. The eigenfrequencies of the 0, 1st and 2nd order 'trapped-leaky' modes at each $n=0(1)\,5$ are given in table 2. The corresponding values of $|A_{nk}|\exp\{-\eta_k\bar{t}\}$ and $|R_n(a_1,t)|$ (table 2) show that, by the time $\bar{t}=10$, the amplitudes of the *almost trapped* modes exceed, not only the corresponding $|R_n(a_1,t)|$, but also $|R_0(a_1,t)|$; by the time $\bar{t}=30$, the amplitudes of the fundamental modes at larger n are even more dominant. Further, no mode corresponding to a *second-system* root of $E(\nu;\,0.25,0.7,n)$ is considered, for the amplitude of such a motion diminishes even more rapidly due to its greater damping rate. Hence, even for moderately large $\bar{t}$, the disturbance at the coast is virtually a sum (of standing waves) of fundamental *almost trapped* modes (3.1); the real time equivalent to a given value $\bar{t}$ follows from the relationship $\nu\bar{t}=\sigma t$.

6. Effect of the Earth's rotation

Longuet-Higgins (1967, § 10) has shown that the effect on the *almost trapped* waves over the limiting cricular sill ($\alpha = 0$), of the Coriolis forces due to the rotation of the Earth, is to split the frequencies of each pair of (identical) modes propagated in opposite directions around the sill. The splitting of frequencies would appear as a slow beat in a record of the waves at a fixed point; numerical computation indicates that the beat period is very large. In this section, we briefly investigate the similar split in frequency for the *almost trapped* waves around the circular island.

With the constant Coriolis forces included in the linearized, shallow-water equations of motion, ζ_i^* must satisfy (e.g. see Longuet-Higgins 1967, § 10)

$$[\nabla^2 + K_i^2]\,\zeta_i^* = 0 \quad (i = 1, 2), \tag{6.1}$$

instead of (2.5), where

$$K_i = (\sigma^2 - f^2)^{\frac{1}{2}}/(gh_i)^{\frac{1}{2}} \quad (i = 1, 2), \tag{6.2}$$

and f is the Coriolis parameter. Further, the influence of the rotation is also present in the boundary conditions to be imposed at the coast and edge; in (2.9) and (2.10), one must substitute

$$\frac{\partial}{\partial r} + \mathrm{i}\left(\frac{f}{\sigma}\right)\frac{1}{r}\frac{\partial}{\partial \theta}, \tag{6.3}$$

in place of $\partial/\partial r$. It follows that, on a uniformly rotating Earth, the expression for the free modes of oscillation of the waters around the island has the same form as (3.1) provided K_i replaces k_i $(i = 1, 2)$, and $A_{11}^{(j)}(\nu)$ is substituted for $H_n^{(j)\prime}(k_1 a_1)$ $(j = 1, 2)$ in the shelf part, where

$$A_{lm}^{(j)}(\nu) \equiv K_l a_m H_n^{(j)\prime}(K_l a_m) - (nf/\sigma)\, H_n^{(j)}(K_l a_m). \tag{6.4}$$

It is easily verified that the corresponding characteristic equation is

$$(h_1/h_2)^{\frac{1}{2}} H_n^{(1)}(K_2 a_2)\,[A_{11}^{(1)}(\nu)\, A_{12}^{(2)}(\nu) - A_{11}^{(2)}(\nu)\, A_{12}^{(1)}(\nu)] - A_{22}^{(1)}(\nu)\,[A_{11}^{(1)}(\nu)\, H_n^{(2)}(K_1 a_2) - A_{11}^{(2)}(\nu)\, H_n^{(1)}(K_1 a_2)] = 0 \quad (a_1 \neq 0). \tag{6.5}$$

Since $|f/\sigma| < 0.1$ even for oscillations with periods as great as 1 h, attention will be focused on those roots of (6.5) where $|f/\sigma| \ll 1$. But equation (6.5) reduces to (3.5) when $f = 0$. Thus, one may anticipate that the roots of (6.5) with $|f/\sigma| \ll 1$ lie near (in the complex plane) those of (3.5). Then, regarding that root of (6.5) near the zero σ_l of (3.5) as a function of f (n, a_1, a_2, h_1 and h_2 held fixed), one can calculate that

$$\left.\frac{\partial \sigma_l}{\partial f}\right|_{f=0} = \frac{n(A+B)}{C} \quad (\alpha \neq 0), \tag{6.6}$$

where

$$A = \epsilon^2 H_n^{(1)}(\epsilon\nu_l)\,[H_n^{(1)}(\alpha\nu_l)\, H_n^{(2)\prime}(\nu_l) - H_n^{(2)}(\alpha\nu_l)\, H_n^{(1)\prime}(\alpha\nu_l)] - \epsilon H_n^{(1)\prime}(\epsilon\nu_l)\,[H_n^{(1)}(\alpha\nu_l)\, H_n^{(2)}(\nu_l) - H_n^{(2)}(\alpha\nu_l)\, H_n^{(1)}(\nu_l)],$$

$$B = \alpha(\epsilon^2 - 1)\, H_n^{(1)}(\epsilon\nu_l)\,[H_n^{(1)\prime}(\alpha\nu_l)\, H_n^{(2)}(\nu_l) - H_n^{(2)\prime}(\alpha\nu_l)\, H_n^{(1)}(\nu_l)],$$

$$C = (n^2 - \alpha^2\nu_l^2)\, A + n^2 B + \epsilon\alpha\nu_l^2(\epsilon^2 - 1)\, H_n^{(1)\prime}(\epsilon\nu_l)\,[H_n^{(1)\prime}(\alpha\nu_l)\, H_n^{(2)\prime}(\nu_l) - H_n^{(2)\prime}(\alpha\nu_l)\, H_n^{(1)\prime}(\nu_l)],$$

and ϵ, α and ν are the dimensionless variables introduced in § 3; the corresponding expression when $\alpha = 0$ can be found by taking the appropriate limit (cf. § 3) of (6.6). Table 1 records the values of the real part of (6.6) for the *almost trapped* modes represented there. They are all positive. It follows that the real part of the root of (6.5) corresponding to the zero ν_k of (3.5) is greater or smaller than ξ_k according as the sign of nf/ξ_k – sgn (nf/ξ_k) – is positive or negative. But positive (negative) sgn (nf/ξ_k) implies that the *almost trapped* mode (3.1) is propagated along the shelf in the same sense as (against) the rotation of the Earth, i.e. with the coast on its left (right)

in the Northern hemisphere; Ball (1967) calls such waves positive (negative). Hence, for those modes with $|f/\sigma| \ll 1$ the positive (negative) *almost trapped* wave motion (3.1) has a greater (smaller) frequency than when the Earth's rotation is not included in the model. Longuet-Higgins (1967) arrives at the same conclusion for the corresponding modes over the circular sill; the same behaviour has already been noted in the edge (trapped) wave modes propagated along a straight coast (see, for example, Reid 1958; Mysak 1968; Munk *et al.* 1970).

Furthermore, the rotation-induced 'beat frequency', $\Delta\xi_k$, between the similar positive and negative kth modes (3.1) is virtually f times the real part of the quantity (6.6). Those values (6.6) recorded in table 1 show that $\Delta\xi_k$ is of order $(h_1/h_2)f/n$ while the island is interior to the mode's

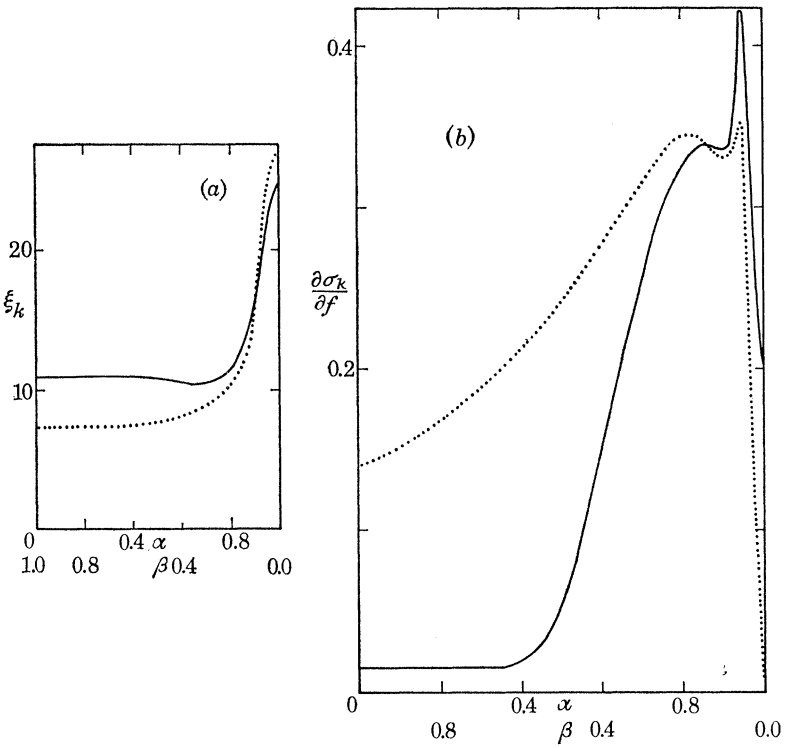

FIGURE 13. Analogy between the modes (3.1) (full curves) and the modes (A 2) (dotted lines) at $n = 7$, $\epsilon = 0.25$. (*a*) The frequency as a function of the shelf (ledge) width; (*b*) the rotation-induced beat frequency (divided by f) as a function of the shelf (ledge) width.

inner critical circle ($\alpha < \alpha_k$, where α_k is defined in (3.20)), of order f/n when $\alpha \doteqdot \alpha_k$, and for $k > 0$, tends to zero as α approaches the mode's cut-off shelf width (where $\xi_k \doteqdot n/\epsilon$); for the fundamental mode, as α approaches 1 (its cut-off shelf width), $\Delta\xi_0$ approaches the real part of $nf/(n^2-\mu_{n0}^2)$, where μ_{n0} is that root of $H_n^{(1)\prime}(\nu)$ nearest to the real axis (figure 4). Figure 13(*a*) demonstrates that the analogy between the gravity waves trapped on the ledge of appendix A and shelf of the model (2.1) is best when n is large and the shelf is relatively narrow ($\alpha \doteqdot 1$, $\beta \doteqdot 0$); figure 13(*b*) shows that the rotation-induced beat frequencies are comparable not only when the respective shelves are wide ($\alpha \doteqdot 0$, $\beta \gg 1$), but also when they are narrow. The analysis of the rotation-induced 'beat-frequency' for the motions on the ledge is given in appendix B.

We also note that equation (6.5) ($f \neq 0$) has real roots characterized by $|\sigma/f| \leqslant 1$ and $nf/\sigma < 0$, i.e. there exist low-frequency, negative, wave motions perfectly trapped around the island; some consideration has been given to them in Summerfield (1969). One limiting case, for the model

where $a_1 = a_2$, has been analysed by Longuet-Higgins (1969), and another limiting case, where the motions are assumed horizontally non-divergent (quasigeostrophic), has been mentioned by Rhines (1969).

7. Cylindrical symmetry; the general case

In § 3, we saw that the presence of the island ($a_1 \neq 0$) on the immobilized underlying sill little affected those trapped wave-modes with inner critical (caustic) circles on the shelf. Also, the analyses of §§ 4, 5 revealed that such modes would not be detected at the shoreline. Thus, in order to generalize the results of the preceding sections to other island-shelf systems displaying

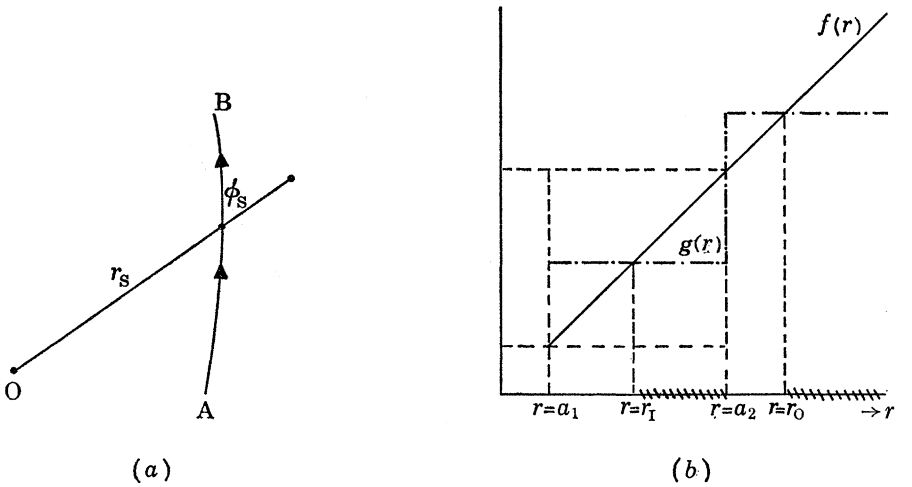

Figure 14. (*a*) Definition diagram for the angle of intersection between the wave ray AB and the position vector at $r = r_s$; (*b*) graphs of $f(r)$ (full line) and $g(r)$ (dashed-dotted line) as functions of r; there exists a real path in the (r, θ) plane for the wave-ray defined by (7.5) when $r_1 \leqslant r \leqslant a_2$ and $r \geqslant r_0$.

cylindrical symmetry, we must first determine whether the possible trapped wave motions can have inner critical circles on the shelf.

It is known that the refraction of waves in water of slowly varying depth obeys Snell's law (see, for example, Sverdrup & Munk 1944). This implies that for those wave trains with small wavelength the path of each wave ray, or orthogonal to the wave fronts, is such that the functional (Fermat's principle of least time; e.g. see, for example, Arthur 1946)

$$\int \frac{\mathrm{d}s}{c}, \tag{7.1}$$

has an extremum. The limits of the integration along the path need not be specified in the present context; $\mathrm{d}s = (r^2 + \dot{r}^2)^{\frac{1}{2}}\,\mathrm{d}\theta$, where $\dot{r} \equiv \mathrm{d}r/\mathrm{d}\theta$, denotes an element of length along the wave-ray at the point where the wave-velocity is c. For island-shelf complexes displaying cylindrical symmetry, the water-depth h is a function of r only. Consequently, $c = (gh)^{\frac{1}{2}} = C(r)$, in which case, the Euler equation for the functional,

$$\frac{\partial}{\partial r}\left\{\frac{(r^2+\dot{r}^2)^{\frac{1}{2}}}{c}\right\} - \frac{\mathrm{d}}{\mathrm{d}\theta}\frac{\partial}{\partial \dot{r}}\left\{\frac{(r^2+\dot{r}^2)^{\frac{1}{2}}}{c}\right\} = 0, \tag{7.2}$$

can be integrated once, yielding $\qquad (\dot{r})^2 = r^2\{(r/cA)^2 - 1\}, \tag{7.3}$

where A is the constant of integration. The latter constant can be computed from the condition that, at $r = r_s$, the angle between the radius vector and the wave ray, ϕ_s, is given by (figure 14*a*)

$$\sin^2\phi_s = r_s^2/(r_s^2 + \dot{r}_s^2). \tag{7.4}$$

On eliminating $\dot{r}_s$ between (7.3) and (7.4), one finds that $A = c_s^{-1} r_s \sin\phi_s$, where $c_s = c(r_s)$. Thus, the path of the wave ray passing through $r = r_s$ is specified by

$$\frac{\mathrm{d}r}{\mathrm{d}\theta} = \pm r\left\{\frac{f^2(r)}{g^2(r)} - 1\right\}^{\frac{1}{2}}, \tag{7.5}$$

where we have written, for convenience,

$$f(r) = r/r_s, \quad g(r) = c_s^{-1} c(r) \sin\phi_s. \tag{7.6}$$

We use the results of § 3 to show how (7.5) determines whether the trapped wave-modes for more general island-shelf complexes have caustic circles on the shelf.

With $h(r)$ given by (2.1), and $a_1 < r_s < a_2$, $g(r) = \sin\phi_s$ when $a_1 < r < a_2$ and $g(r) = \epsilon^{-1}\sin\phi_s$ when $r > a_2$, where ϵ is defined by (3.9). From (7.6), one can calculate that $g(r) = f(r)$ when $r_I = r_s \sin\phi_s$ and $r_O = r_s \epsilon^{-1} \sin\phi_s$; r_I and r_O exist ($a_1 < r_I \leqslant r_s$, $r_O > a_2$) provided r_s and ϕ_s are suitably chosen (figure 14(*b*)). On the other hand, r_I and r_O are the radii of, respectively, the inner and outer critical circles of any mode (3.1) (n large) satisfying the condition (7.4) at $r = r_s$ (see § 3); equation (7.5) describes the path (straight lines) of each wave ray of the mode. In other words, regions of the (r, θ) plane where $g(r) < f(r)$ in (7.5) ($\mathrm{d}r/\mathrm{d}\theta$ real) correspond to 'wave' domains for the mode, and regions where $g(r) > f(r)$ ($\mathrm{d}r/\mathrm{d}\theta$ complex) are either interior to the inner critical circle, or are between 'wave' domains (figure 14*b*). On applying this interpretation of (7.5) to the motions of the waters about other island-shelf systems displaying cylindrical symmetry, one sees that for those models where the depth of water is zero at the coast† all trapped wave modes have 'wave' domains adjacent to the coast [$g(a_1) = 0$] (cf. Shen *et al.* 1968). Whether critical circles do exist between the coast and the edge depends very much on the form of $h(r)$; if such circles should exist then the outermost one is the inner critical circle in the present terminology. Also, if the ocean is of finite depth at large distances from the island, $g(r)$ approaches a finite-valued constant for large r, and so must ultimately be less than $f(r)$. It follows that all modes have 'wave' domains at large distances from the island, i.e. they all 'leak' energy to the ocean, as has already been predicted (Longuet-Higgins 1967) by other arguments.

The α-curve method of computation for the eigenfrequencies of the trapped wave-modes (3.1) disclosed that there exist two types of oscillation for the model (2.1), namely 'trapped-leaky' and 'shelf-island' motions. The latter modes were seen to be little influenced either by the size of the island on the (immobilized) underlying sill or by the depth of water on the shelf, and their contributions to the disturbances excited in the shallow-water region by radiation incident on the edge from the ocean were negligible. Thus, although we can expect similar modes to exist for other island-shelf systems displaying cylindrical symmetry, they will not play an important role in the shelf dynamics. On the other hand, the response of the shelf of the model (2.1) to the external radiation incident on the edge is dominated by that of the fundamental modes at each n, the magnitude and duration of the disturbance being determined by the magnitudes of the damping factors of these modes. The damping factors are themselves critically dependent on the relative depths of the water at the edge, and on the size of the island relative to that of the underlying sill. The first dependence stems from the sensitivity of the 'topographically induced' energy dissipation

† The boundary condition to be applied at the shoreline for 'edge' or 'trapped' wave modes now requires that the amplitude of the motion be finite there (Reid 1958; Smith 1970).

PHILOSOPHICAL TRANSACTIONS OF THE ROYAL SOCIETY A MATHEMATICAL, PHYSICAL & ENGINEERING SCIENCES

for the mode, on the amount by which the angle of incidence (3.4) at the edge (of the mode's shelf components) exceeds the critical angle, and the later dependence results from the influence on (3.4) of the width of the shelf. Further, the limiting case of the vertical-walled island standing in water of constant depth shows that the fundamental modes always have finite eigenfrequencies. Hence, for other island-shelf complexes displaying cylindrical symmetry, we anticipate that the fundamental modes have small damping factors only if the continental slope region is very steep, and the shelf, broad (cf. Shen *et al.* 1968); indeed, we can expect *almost trapped* modes only for those isolated islands with a 'hedge region' (Longuet-Higgins 1967, § 9), where h increases at least as fast as r^2. In other words, for the three islands depicted in figure 15, we expect every fundamental

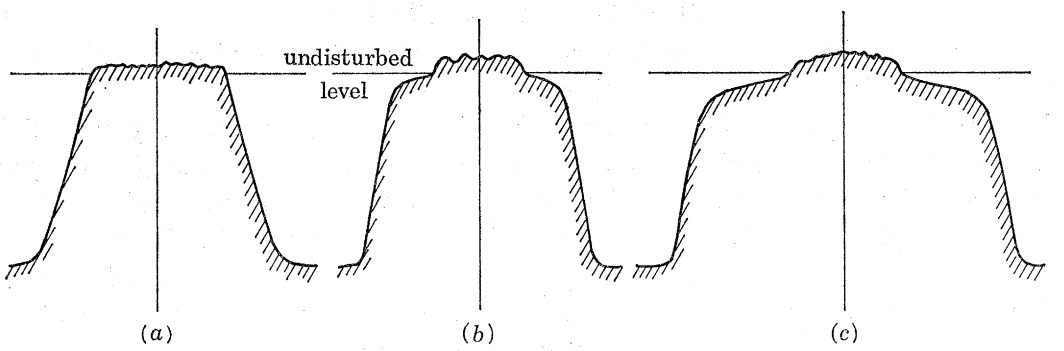

FIGURE 15. Meridional sections of islands displaying cylindrical symmetry: (*a*) concave continental slope; (*b*) convex, narrow continental shelf; (*c*) convex, broad continental shelf.

trapped-wave mode of (*a*) to be more heavily damped than the corresponding mode of (*b*) which, in turn, will be more heavily damped than the corresponding mode of (*c*). Finally, I do not consider the influence of the different topographies on the higher-order 'trapped-leaky' modes at each n, for these modes play a minor role in the dynamics of the water region over the shelf.

These ideas concerning the influence of the shelf topography on the various fundamental trapped wave-modes are consistent with the results of previous theoretical studies on the amplification of shallow-water waves at circularly symmetric islands. For example, Webster & Perry (1966) (also see Adams 1969) have computed the amplitude of the disturbance at the bow of the island (the point $\theta = 180°$ in § 4), caused by the incidence of simple-harmonic plane-wave radiation on the island-shelf complex from the ocean; they calculate the response as a function of the frequency of the incident waves, for various values of both the curvature of the sloping shelf and of the ratio of the radius of the island at sea level to that at the sea floor. We anticipate peaks in each amplitude response curve when the frequency ν_b ($= 2\pi r_b/\lambda$, where λ = wavelength of incident waves, r_b = radius of island at sea floor) of the incident waves satisfies a condition similar to (4.10), where ξ_k is the frequency of a fundamental mode for the complex; as ν_b increases the peaks will correspond, respectively, to the fundamental mode at $n = 1, 2, \ldots$. Moreover, the maximum value of each peak will be inversely proportional to the rate of damping of the mode, whereas the width of the peak will be directly proportional to the same quantity. The graphs o Webster & Perry (1966) verify that the maxima are small (large) both when the slope is concave (convex) (as in, respectively, figures 15*a*, *c*) and when the shelf region is narrow (wide). In interpreting the graphs, we must remember that some modes have caustic circles on the shelf and so will hardly be detected at the shoreline, and that, for those models where the slope is convex and the shelf wide, the eigenfrequencies of the 'trapped-leaky' modes at a given value of n are close together (see Summerfield 1969, § 6.5) causing the peaks to be much broader.

It is now clear that the coastline amplitude response curves (to sinusoidal long-wave radiation from uniform depth oceans) which have been computed for several simple island-shelf models (Omer & Hall 1949; Homma 1950; Lautenbacher 1970) should be explained in terms of the excitation of trapped wave-modes by the incident wave trains. Such an interpretation not only clarifies the origin of the 'peaks' and 'valleys' in graphs of maximum wave amplitude versus angular position (e.g figure 10) commented on by Lautenbacher (1970) (also see Homma 1950; Vastano & Reid 1967), but also reveals how one can determine the frequencies at which large responses will be observed. One has only to compute the eigenfrequencies of the fundamental trapped wave-modes for the system.

8. Further discussion; an application

In the previous sections, we have neglected, among other things, the effect on the trapped wave-modes of other forms of energy loss, such as that due to viscous (laminar or turbulent) damping. This latter question has been considered by Longuet-Higgins (1967, §§ 11, 12), and his conclusions apply to the motions around our island-shelf complex. For the *almost trapped* modes (3.1), the dissipation of energy by viscous effects will exceed that due to the nature of the topography. Thus, although we might still expect the coastline amplitude response function (4.8) to be dominated by the one mode (3.1) under the conditions specified in § 4, the observed amplitudes will be much smaller than predicted.

There have been reported in the literature several laboratory studies on the amplification of long waves by circular islands (see, for example, Weiner 1947; Laird 1935; Wong *et al.* 1963). None has specifically sought to verify the existence of trapped wave-modes. Nevertheless, we note that Williams & Kartha (1969; figure 11) observed on one occasion a large amplitude response (at the coast) with virtually a $\cos\theta$ dependence in the azimuthal direction, and also, that they verified Homma's (1950) theoretical, coastline amplitude response curve for the one model where all the necessary parameters were identical. Such results tend to substantiate our interpretation of the shelf disturbance in terms of the excitation of trapped wave-modes.

Probably the most important effect which we have neglected up to date is the influence on the trapped wave-modes of deviations in the bottom topography from the perfect symmetry considered here. Shen *et al.* (1968) did not raise this question. On the other hand, Longuet-Higgins (1967, § 9) pointed out that trapped wave-modes may exist for any isolated feature raised from the sea floor provided there is at least one complete refraction path around it. The latter author also showed that a small perturbation in the topography from the cylindrical symmetry of his model may cause similar modes to have slightly different frequencies; the combined motions would then produce a 'topographically-induced' beat in a record of the waves at a fixed point, similar to the 'rotation-induced' beat examined in § 6. Summerfield (1969) investigated the 'topographic' beat by computing the eigenfrequencies of the trapped wave-modes for a model elliptic seamount, similar to Longuet-Higgins's model circular sea-mount. He found that a large beat might be expected, even when the length of the major axis of the feature only exceeds that of the minor axis by as little as 25 %. Summerfield concluded that the 3 h 'beat' in the 6 min period wave-phenomenon discovered in wave records from Macquarie Island (54° 30′ S, 158° 58′ E), which initiated Longuet-Higgins's original study, may well be due to the contouring of the sea floor about the island.

In the study of sound scattering by cylinders, where the cylinder's generators are normal to the

PHILOSOPHICAL TRANSACTIONS OF THE ROYAL SOCIETY A MATHEMATICAL, PHYSICAL & ENGINEERING SCIENCES

plane of the incident waves, the magnitude of the parameter ka determines whether there is weak forward scattering ($ka < 1$) or pronounced back-scattering with strong shadowing on the lee side ($ka > 1$); k is the wave-number of the incident waves and a is the radius of the cylinder. Regarded as a scatterer of the wave-trains (4.1), the island-shelf system (2.1) hardly perturbs those oscillations where $ka = ka_2 = \epsilon\nu < 1$; the large amplitude resonances of the shelf, which can be excited provided (4.10) is satisfied, correspond to $1 < \epsilon\nu < 5$ (see § 3). Thus, we might expect the wave record from a gauge fixed at the coast to be relatively free from the distortion of shelf oscillations for those wave motions (4.1) with periods greater than 15 min ($a_2 = 30$ km, $h_2 = 4$ km) (cf. Van Dorn 1970).

Finally, let us examine the power spectra of consecutive, equal length pieces of wave record made at the coast after the passage of the straight line-pulse (5.1), i.e. seek the characteristics of spectra of the disturbance (5.11). Suppose that each section of record is of length T; then the midpoints of the successive pieces subjected to spectral analysis are $t = \frac{1}{2}T + t_0, \frac{3}{2}T + t_0, \ldots$ where $t_0 (\geqslant 0)$ is a constant. Ignoring the transient tails in (5.11) for the moment, one can calculate that each free mode (3.1) contributes to the spectral density function of the pth record ($p = 1, 2, \ldots$) an amount proportional to

$$\tfrac{1}{2}\gamma_n^2 \cos^2 n\theta |\Lambda_{nl*}|^2 \exp\{-\eta_{l*}(2p-1)\,\overline{T}\}\,\mathrm{d}\nu, \tag{8.1}$$

in the interval $|\nu - \xi_{l*}| < 0.5\,\mathrm{d}\nu$, where $\overline{T}$ is defined in the same way as $\bar{t}$ in (5.4). Thus, provided the spectra are computed at successive frequencies whose separation is less than that between the frequencies of the successive fundamental ($n = 1, 2, 3, \ldots$) trapped wave-modes (3.1), the consecutive spectra exhibit a decrease in energy at each frequency, coupled with increasing resolution of the 'peaks' due to the rapid decay of all but the fundamental *almost trapped* modes. Furthermore, the sequence of spectra for different directions of travel of the line pulse resemble one another, with slight discrepancies resulting from the cosine dependence in (8.1). On the other hand, spectra from different islands for the same line pulse are dissimilar because the eigenfrequencies of the respective *almost trapped* modes are not identical. These features can be seen in the spectra of real wave records made following the passage of a tsunami (see, for example, Loomis 1966, figures 3, 4, 14) which intimates that the interaction between tsunamis and small islands might be explained in terms of the excitation of trapped wave motions; we note that the rotation-induced split in frequency between the similar positive and negative (§ 6) trapped wave-modes is below the limit of detection in Loomis's spectra. This agreement with observation also confirms that the contributions of the transient tails $|R_n(a_1, t)|$ to the theoretical spectra are negligible provided t_0 is sufficiently large.

Lastly, if the implied interpretation of the interaction between tsunamis and small islands is correct, then we can see why tsunamis are not amplified at steep-sided islands. For these features, the fundamental trapped wave-modes have large damping factors. It follows that the shallow water disturbance will be of small amplitude, and will be rapidly dissipated after the tsunami has passed.

Appendix A. Straight shelf investigation

Let x and y be horizontal Cartesian coordinates in the plane, undisturbed water surface. The depth function (figure A 1)

$$h(r, \theta) \to h(x, y) = \begin{cases} h_1, & -a < x < 0, \\ h_2, & x > 0, \end{cases} \tag{A 1}$$

where $a(>0)$, h_1 and $h_2(>h_1)$ are constants, models a shelf of uniform width a, bordered by a straight coast along $x=-a$, and a straight edge along $x=0$. This shelf region will be referred to as the *ledge*, in order to distinguish it from that around the circular island.

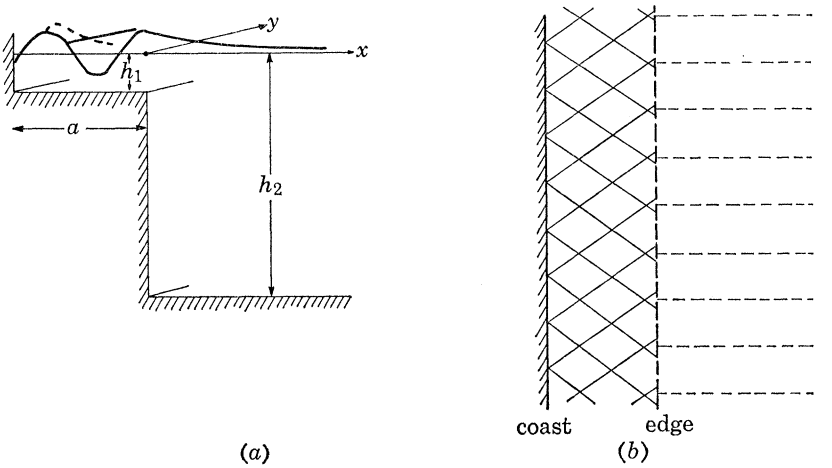

FIGURE A 1. The straight ledge, and its trapped wave motions: (*a*) section normal to the coast; (*b*) plan view of wave crests (full lines).

In the present context, the most appropriate form of the expression for the wave motions trapped on the ledge is (the real part of)

$$\zeta(x,y,t) = A\exp\{\mathrm{i}(my-\sigma t)\}\begin{cases} R\exp\{\mathrm{i}(l_1x+\gamma)\}+R\exp\{-\mathrm{i}(l_1x+\gamma)\} & (-a<x<0) \\ \exp\{-l_2x\} & (x>0), \end{cases} \tag{A 2}$$

where the differential equations (2.5) require that

$$l_1^2 = \sigma^2/gh_1 - m^2, \quad l_2^2 = m^2 - \sigma^2/gh_2, \tag{A 3}$$

and the boundary conditions (2.8), (2.9), (2.10), that

$$\gamma = \arctan(h_2l_2/h_1l_1), \quad R = \tfrac{1}{2}[1+(h_2l_2/h_1l_1)^2]^{\frac{1}{2}}, \tag{A 4}$$

and

$$l_1\tan al_1 = (h_2/h_1)\,l_2. \tag{A 5}$$

Provided σ, m, l_1 and $l_2(>0)$ are all real, the expression (A 2) represents a wave motion propagated along the coast and virtually confined to the ledge. The solution is illustrated in figure A 1. The trapping of the motion on the ledge is essentially due to the train of waves

$$AR\exp\{\mathrm{i}(l_1x+my-\sigma t+\gamma)\} \tag{A 6}$$

propagated towards the ocean at the speed $(gh_1)^{\frac{1}{2}}$ of long waves in shallow water of uniform depth h_1, meeting the edge at an angle of incidence $\phi_1[=\arcsin m(gh_1)^{\frac{1}{2}}/\sigma]$ which exceeds the critical angle, $\phi_c[=\arcsin(h_1/h_2)^{\frac{1}{2}}]$ for the depth function (A 1) (Longuet-Higgins 1967, § 3). The waves are internally totally reflected from the edge, the reflected waves being given by

$$AR\exp\{\mathrm{i}(-l_1x+my-\sigma t-\gamma)\}. \tag{A 7}$$

In turn, the latter are perfectly reflected from the coast into the waves (A 6). Only an 'exponential fringe' of radiation appears on the ocean side of the edge.

It will shortly be seen that the characteristic equation (A 5) has a discrete, non-empty set of real roots for every non-zero a and m. For the present moment, we note that the equation can

also be obtained by equating to an integral multiple of 2π, the total phase-change in the waves (A 6) and (A 7) which occurs when the ledge is normally crossed and recrossed (y and t held constant) (cf. waveguide mode theory; see, for example, Budden 1961).

In this investigation of the wave-motions (A 2), we examine those modes with the same along-edge wavenumbers as the modes (3.1), i.e. we set

$$m = n/a_2, \tag{A 8}$$

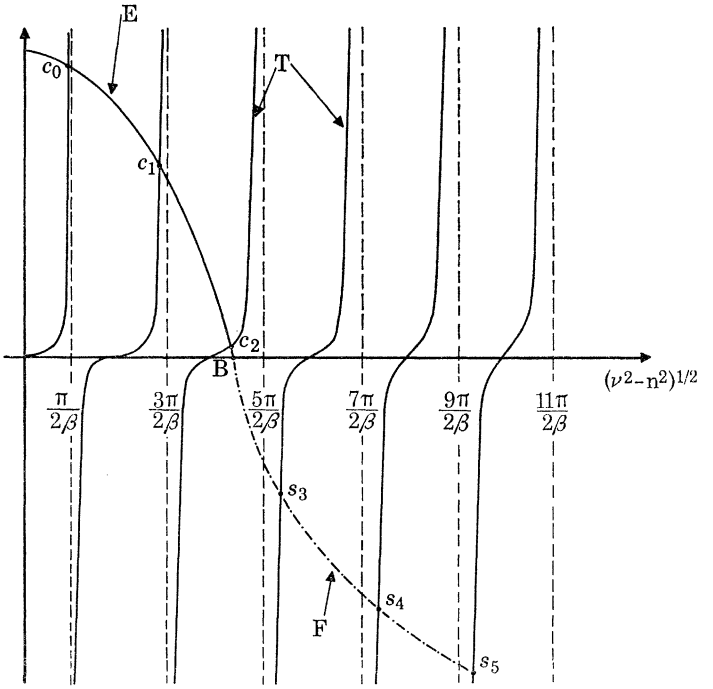

FIGURE A 2. Representative graphs of $(\nu^2-n^2)^{\frac{1}{2}}\tan\beta(\nu^2-n^2)^{\frac{1}{2}}$ (labelled T), $\epsilon^{-2}(n^2-\epsilon^2\nu^2)^{\frac{1}{2}}$ (E) and $-D\epsilon^{-2}(\epsilon^2\nu^2-n^2)^{\frac{1}{2}}$ (F) as functions of $(\nu^2-n^2)^{\frac{1}{2}}$. The eigenfrequencies of the trapped and leaky modes (A 2) are given by the abscissae of, respectively, the finite set of points $\{c_0, c_1, c_2\}$ and the infinite set $\{s_3, s_4, s_5, \ldots\}$. B is the point $[n(1-\epsilon^2)^{\frac{1}{2}}/\epsilon, 0]$.

where a_2 is the radius of the underlying sill of the model (2.1). It follows from (A. 3) that

$$a_2 l_1 = (\nu^2-n^2)^{\frac{1}{2}}, \quad a_2 l_2 = (n^2-\epsilon^2\nu^2)^{\frac{1}{2}}, \tag{A 9}$$

where ν and ϵ are the dimensionless quantities defined, respectively, in (3.8) and (3.9). Thus, provided that we specify

$$\beta = a/a_2, \tag{A 10}$$

as the dimensionless width of the ledge, the eigenfrequencies of the perfectly trapped modes (A 2) are the real roots of

$$L(\nu;\epsilon,\beta,n) \equiv (\nu^2-n^2)^{\frac{1}{2}}\tan\beta(\nu^2-n^2)^{\frac{1}{2}} - \epsilon^{-2}(n^2-\epsilon^2\nu^2)^{\frac{1}{2}}. \tag{A 11}$$

The parameter β has the range $0 < \beta < \infty$ in contrast with that of α; further, small (large) β corresponds to a narrow (wide) ledge.

Figure A 2 reveals that L has one real root, ν_k, in the interval

$$k\pi/\beta < (\nu^2-n^2)^{\frac{1}{2}} < (k+\tfrac{1}{2})\pi/\beta \quad (k = 0, 1, 2, \ldots) \tag{A 12}$$

whenever $k\pi/\beta < n(1-\epsilon^2)^{\frac{1}{2}}/\epsilon$, i.e. when

$$\beta > k\pi\epsilon/n(1-\epsilon^2)^{\frac{1}{2}} = \beta_k, \quad \text{say.} \tag{A 13}$$

The x-component of the corresponding mode (A 2) has k zeros in $-a < x < 0$, i.e. the trapped wave motion has k nodal lines parallel to the coast on the ledge; it will be designated the kth mode. Further, β_k will be known as the cut-off ledge width for the kth mode.

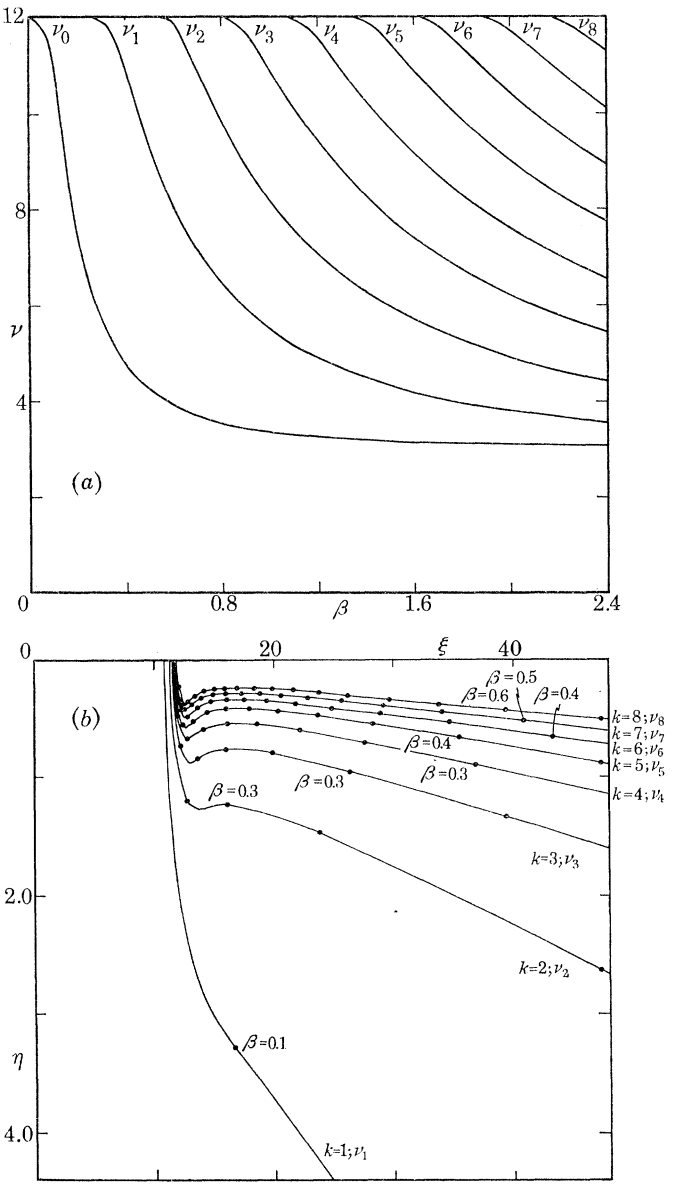

FIGURE A 3. The roots of $L(\nu; 0.25, \beta, 3)$ as functions of the ledge width β. (*a*) Real zeros in the interval $(0, 2.4)$; there exist 8 curves because, according to (A 13), there are 8 cut-off ledge widths less than 2.4 (multiples of 0.2704). (*b*) Complex zeros corresponding to $k = 1(1)8$ in (A 14); β decreases to the right on each curve and the heavy dots are spaced at intervals of 0.1 in β.

We seek the changes in the kth mode (A 2), of fixed wavenumber n along the edge, caused by decreasing the width β of the ledge to zero (ϵ held fixed); they can be determined from the various relations (A 9) once the dependence of ν_k on β is known. With n and ϵ held fixed, β_k is a constant, and the curve labelled E in figure A 2 is a fixed curve. From figure A 2, it is easily seen that, as β approaches β_k from ∞, the value of ν_k increases from n to n/ϵ, and the angle of incidence at the

edge of the mode's shelf-components decreases from $\frac{1}{2}\pi$ to ϕ_c; the components (A 6) and (A 7) turn at such a rate that the phase-change incurred in the crossing of the ledge compensates the decreasing width of the latter. When $\beta < \beta_k$, the real root ν_k does not exist. However, the foregoing analysis indicates that as β is decreased through β_k, the wave components (A 6) and (A 7) will continue to turn, in which case, the former will be incident at the edge at an angle less than ϕ_c. It follows that there must be a refracted wave in the ocean propagated away from the edge. Thus, the mode 'leaks' energy from the ledge to the ocean. Consequently, the motion must decay in time; ν_k will be complex with negative imaginary part. By use of the *step-by-step* method of numerical computation, it is easily verified that there does exist such a root ν_k of L for $\beta < \beta_k$ with negative imaginary part η_k, and with real part, ξ_k, approaching n/ϵ as β approaches β_k from below. Furthermore, when β goes to zero,

$$\nu_k \sim \frac{(k-\frac{1}{2})\pi}{\beta} - \mathrm{i}\frac{\operatorname{arctanh}\epsilon}{\beta} \quad (k \geqslant 1); \tag{A 14}$$

the right-hand values are the large ($|\epsilon\nu| \gg n$) analytical zeros of L. Figure A 3 plots the *β-curves* of the roots ν_k of $L(\nu;\ \epsilon = 0.25, \beta, n = 3)$ for $k = 0(1)\ 8$. Finally, the numerical calculations reveal that for $\beta < \beta_k$, ξ_k is virtually given by the root of

$$(\nu^2-n^2)^{\frac{1}{2}} \tan\beta(\nu^2-n^2)^{\frac{1}{2}} = -D\epsilon^{-2}(\epsilon^2\nu^2-n^2)^{\frac{1}{2}}, \tag{A 15}$$

where $|(\nu_k^2-n^2)^{\frac{1}{2}} - k\pi/\beta| < \pi/2\beta$ (see Summerfield 1969); D is an arbitrary positive constant. The curve labelled F in figure A 2 represents the right-hand side of (A 15)

Hence we see that, on any ledge, the modes (A 2) of fixed wavenumber n along the edge have the property that

$$\nu_0 < \nu_1 < \ldots < \nu_j < \xi_{j+1} < \xi_{j+2} < \ldots, \tag{A 16}$$

where the jth mode is the highest-order perfectly trapped motion, i.e. j is the largest k of (A 13) for which the cut-off ledge width is less than the actual width of the ledge. When the latter is decreased, the jth mode ($j = k, k-1, \ldots, 1$) changes in character from a perfectly trapped wave to a 'leaky wave' as β decreases through β_j; for $\beta \ll \beta_j$, ν_j is given by (A 14). Thus, when the width of the ledge is such that $\beta < \beta_1$ the only trapped mode which can exist is the fundamental. In the limit $\beta = 0$ this mode has the finite frequency n/ϵ, which depends on the wavenumber along the edge, and depth parameter ϵ. This contrasts with the limiting behaviour for all the higher order modes, as given by (A 14); the limit frequency depends only on the mode order. However, the limit trapped wave frequency for these latter modes is n/ϵ at their respective cut-off ledge widths (A 13).

Appendix B. The rotation-induced 'beat-frequency'

On a uniformly rotating earth, the characteristic equation for the trapped wave-modes on the ledge (A 1) is (Summerfield 1969)

$$l_1 \tan al_1 - \frac{h_2}{h_1} l_2 = \frac{mf}{\sigma}\left[\frac{h_2}{h_1} + \frac{h_2 l_2}{h_1 l_1}\tan al_1 + \frac{mf}{\sigma}\frac{(h_2-h_1)}{h_1 l_1}\tan al_1\right], \tag{B 1}$$

where

$$l_1^2 = (\sigma^2-f^2)/gh_1 - m^2, \quad l_2^2 = m^2 - (\sigma^2-f^2)/gh_2, \tag{B 2}$$

and m, a, h_1 and h_2 are defined in appendix A. Equation (B 1) reduces to (A 5) when $f = 0$.

One finds that the expression for the small change in the frequency of the kth ledge wave-mode (A 2) when $f \neq 0$, analogous to (6.6), is

$$\left.\frac{\partial\sigma_k}{\partial f}\right|_{f=0} = \frac{n}{\nu_k^2[\epsilon^2(n^2-\epsilon^2\nu_k^2)^{-\frac{1}{2}} + \beta(1+\epsilon^2-\epsilon^2\nu_k^2 n^{-2})]}, \tag{B 3}$$

where n, ϵ, β and ν_k are the dimensionless variables of appendix A. Since the square-bracketed term in (B 3) is positive for $n < \nu_k < n/\epsilon$, it follows that the root of (B 1) ($f \neq 0$) near the real root σ_k of (A 5) is, in general, real, and is greater or less than σ_k (in magnitude) according as sgn (nf/σ_k) is positive or negative. In other words, the positive (negative) perfectly trapped wave-motion (A 2) has a greater (smaller) frequency than when the Earth's rotation is not included in the

TABLE A 1. ACCURATE VALUES OF THE FREQUENCIES AND ROTATION-INDUCED BEAT FREQUENCIES (DIVIDED BY f) OF THE FUNDAMENTAL LEDGE WAVE-MODES (A 2) AT $n = 1, 3, 5, 7$, WHEN $\epsilon = 0.25$

n / β	1		3		5		7	
	ν_0	(B 3)	ν_0	(B 3)	ν_0	(B 3)	ν_0	(B 3)
0.01	3.9998	0.0094	11.9952	0.0282	19.9776	0.0473	27.9372	0.0669
0.02	3.9993	0.0188	11.9804	0.0571	19.9044	0.0975	27.7149	0.1415
0.04	3.9972	0.0377	11.9142	0.1190	19.5039	0.2157	26.1571	0.3137
0.06	3.9935	0.0571	11.7743	0.1900	18.3730	0.3310	22.2743	0.3482
0.08	3.9881	0.0769	11.5033	0.2678	16.3475	0.3514	18.4990	0.3301
0.10	3.9809	0.0975	11.0238	0.3310	14.2713	0.3355	15.8181	0.3285
0.20	3.9008	0.2157	7.5558	0.3284	8.8841	0.3388	10.2555	0.3409
0.40	3.2695	0.3514	4.7762	0.3422	6.2813	0.3178	7.9830	0.2734
0.60	2.5186	0.3284	3.9214	0.3276	5.6183	0.2626	7.4597	0.2082
0.80	2.0594	0.3317	3.5572	0.2958	5.3602	0.2160	7.2641	0.1647
1.00	1.7768	0.3388	3.3710	0.2628	5.2350	0.1812	7.1709	0.1353
2.00	1.2563	0.3178	3.0990	0.1552	5.0605	0.0971	7.0435	0.0703
3.00	1.1237	0.2626	3.0447	0.1073	5.0271	0.0657	7.0194	0.0472
4.00	1.0721	0.2160	3.0253	0.0816	5.0153	0.0496	7.0110	0.0355
5.00	1.0470	0.1812	3.0163	0.0657	5.0098	0.0398	7.0070	0.0285
10.00	1.0121	0.0971	3.0041	0.0332	5.0025	0.0200	7.0018	0.0143

model. Furthermore, the rotation-induced 'beat-frequency' $\Delta\sigma_k$ between the positive and negative kth modes of the same along-edge wavenumber m is virtually f times the quantity (B 3). The latter expression clearly shows that, regarded as a function of β (n, ϵ and k held fixed), $\Delta\sigma_k$ has the properties

$$\lim_{\beta\to\infty} \Delta\sigma_k = \frac{b}{n\beta}(\nu_k \to n); \quad \lim_{\beta\to\beta_k^+} \Delta\sigma_k = 0(\nu_k \to n/\epsilon), \tag{B 4}$$

where β_k is the mode's cut-off ledge width (A 13). The values of (B 3) in table A 1 demonstrate these properties for the fundamental ($k = 0$) mode; note that $\beta_0 = 0$. Some further effects of the Coriolis forces on the trapped ledge wave-modes are described in Summerfield (1969).

We also note that, besides the zeros corresponding to the positive and negative inertio gravity-waves (A 2), equation (B 1) ($f \neq 0$) has another real root, where $mf/\sigma < 0$, and, in general, $|\sigma/f| < 1$, which does not have an analogue in (A 5). In the limit $a = \infty$, the latter zero corresponds to the double Kelvin wave (Longuet-Higgins 1968), of wavenumber m along the edge, trapped along the discontinuity in depth between the oceans of uniform depths h_1 and h_2. One can infer the influence on the double Kelvin wave of the shallower water being of finite extent in the direction normal to the edge, by tracing this root in (B 1) as a is decreased (m, f, h_1 and h_2 held fixed). There results a simple relation, which will be presented in a future paper, between continental shelf wave (e.g. Robinson 1964; Mysak 1967), Kelvin wave (Thomson 1879) and double Kelvin wave motions (Longuet-Higgins 1968). Munk *et al.* (1970, § 4.3) have analysed the motions for the case where m is variable (a, f, h_1 and h_2 held fixed).

Part of this work was incorporated in the author's Ph.D. thesis, done at the Horace I Centre, The Flinders University of South Australia, under Professor J. R. M. Radok; the a acknowledges the support given by a C.S.I.R.O. postgraduate studentship during that pe The research was completed at The Johns Hopkins University under contract N0001 A-0163-000, with the aid of many helpful suggestions from Professor O. M. Phillips, F.R.S author also acknowledges the error in interpretation pointed out by a referee.

Contribution no. 166 of the Chesapeake Bay Institute of The Johns Hopkins University

References

Abramowitz, M. & Stegun, I. A. 1965 *Handbook of mathematical functions*. Dover.
Adams, W. M. 1969 *Hawaii Inst. Geophys. Rep.* no. HIG-69-9.
Arthur, R. S. 1946 *Trans. Am. geophys. Un.* **27**, 168.
Ball, F. K. 1967 *Deep sea Res.* **14**, 79.
Bartholomeusz, E. F. 1958 *Proc. Camb. Phil. Soc.* **54**, 106.
Buchwald, V. T. 1969 *Proc. R. Soc. Lond.* A **308**, 343.
Budden, K. G. 1961 *The wave-guide mode theory of wave propagation*. Logos.
Garipov, R. M. 1965 *Soviet Phys. Dokl.* **10**, 194.
Homma, S. 1950 *Geophys. Mag.* **21**, 199.
Keller, J. B. 1958 *J. Fluid Mech.* **4**, 607.
Laird, A. D. K. 1935 *Trans. Am. geophys. Un.* **36**, 279.
Lautenbacher, C. C. 1970 *J. Fluid Mech.* **41**, 655.
Longuet-Higgins, M. S. 1967 *J. Fluid Mech.* **29**, 781.
Longuet-Higgins, M. S. 1968 *J. Fluid Mech.* **31**, 417.
Longuet-Higgins, M. S. 1969 *J. Fluid Mech.* **37**, 773.
Loomis, H. G. 1966 *Bull. seism. Soc. Am.* **56**, 697.
Munk, W., Snodgrass, F. & Gilbert, F. 1964 *J. Fluid Mech.* **20**, 529.
Munk, W., Snodgrass, F. & Wimbush, M. 1970 *Geophys. Fluid Dynamics* **1**, 161.
Mysak, L. A. 1967 *J. mar. Res.* **25**, 205.
Mysak, L. A. 1968 *J. mar. Res.* **26**, 24.
Olver, F. W. J. 1954 *Phil. Trans. R. Soc. Lond.* A **247**, 328.
Omer, G. C. & Hall, H. H. 1949 *Bull. seism. Soc. Am.* **39**, 257.
Reid, R. O. 1958 *J. mar. Res.* **16**, 109.
Rhines, P. B. 1969 *J. Fluid Mech.* **37**, 191.
Robinson, A. R. 1964 *J. geophys. Res.* **69**, 367.
Shen, M. C., Meyer, R. E. & Keller, J. B. 1968 *J. Phys. Fluids* **11**, 2289.
Smith, R. 1970 *Phil. Trans. R. Soc. Lond.* A **268**, 289.
Snodgrass, F. E., Munk, W. H. & Miller, G. R. 1962 *J. mar. Res.* **20**, 3.
Summerfield, W. 1969 Ph.D. thesis, The Flinders University of South Australia.
Sverdrup, H. U. & Munk, W. H. 1944 *U.S. Navy Dep., Hydro. Office Public.* no. 234.
Thomson, W. 1879 *Proc. R. Soc. Edinb.* **10**, 92.
Van Dorn, W. G. 1970 *J. mar. Res.* **28**, 336.
Vastano, A. C. & Reid, R. O. 1967 *J. mar. Res.* **25**, 129.
Webster, D. L. & Perry, B. 1966 *Stanford Univ. Tech. Rep.* no. 67.
Weiner, F. 1947 *J. acoust. Soc. Am.* **19**, 444.
Williams, J. A. & Kartha, T. D. 1969 *Bull. seism. Soc. Am.* **59**, 299.
Wong, K. K., Ippen, A. F. & Harlemann, D. R. F. 1963 *M.I.T. Tech. Hydro. Lab. Rep.* no. 62.

PHILOSOPHICAL TRANSACTIONS OF THE ROYAL SOCIETY A MATHEMATICAL, PHYSICAL & ENGINEERING SCIENCES